



PROMPT

UCPM-2022-PP/G.A-101101263

Work package 3 Del. Number D3.2

REPORT ON THE IMPLEMENTATION OF THE NUMERICAL MODELS

WP No	Del Rel. No	Del . No	Title	Description	Lead Benefi ciar y	Nature	Disse minati on level	Est.Del. Date
WP 3	D.3.2	D.7	Report on the impleme ntatio of the numerica l models	Models implementatio n, model validation	UGE	Public Report	Public	31 October 2024



UCPM-2022-PP/G.A-101101263-PROMPT



Summary

1. INTRODUCTION	5
1.1. Study Areas	6
1.2. General Methodology	8
2. METOCEAN MODELLING	11
2.1. Hydrodynamic modelling	11
2.1.1. Model description	11
2.1.2. Model application	13
2.2. Atmospheric modelling	19
2.2.1. Model description	19
2.2.2. Model description	19
2.2.3. Model application	22
3. POLLUTION MODELLING: OIL AND CHEMICAL SPILLS	24
3.1. General framework for pollution risk assessment	24
3.2. Marine pollution modelling	25
3.2.1. Model description (TESEO)	26
3.2.1.1. Transport and Dispersion	26
3.2.1.2. Weathering processes for Oil spills	28
3.2.1.3. Weathering processes for HNS spills	30
3.2.2. Model implementation in Genoa	33
3.2.3. On-demand forecast modelling	34
3.2.4. Risk assessment methodology	37
3.2.4.1. Hazard	38
3.2.4.2. Vulnerability	48
3.2.4.3. Risk	50
3.2.4.4. Results	52
3.3. Atmospheric pollution modelling	56
3.3.1. Model description	56
Deposition and Removal Processes	59





3.3.2.	Model implementation	59
	Generation of Meteorological Input Files	59
	Simulation Runs and Postprocessing	60
3.3.2.1.	Coupling between TESEO and HYSPLIT	60
3.3.3.	On-demand forecast modelling	60
3.3.4.	Risk assessment methodology	62
3.3.4.1.	Hazard.....	62
3.3.4.2.	Vulnerability.....	63
3.3.4.3.	Risk.....	63
3.3.4.4.	Results.....	63
4.	REFERENCES.....	64

List of figures

Figure 1	Plan view of the Genoa harbor’s computational domain.....	6
Figure 2	Plan view of the Tripoli harbor’s computational domain.....	7
Figure 3	Plan view of the Aqaba harbor’s computational domain.....	7
Figure 4	- General framework of the system.....	9
Figure 5	- Features of the system implemented by site.	10
Figure 6	On top: high resolution regular grid; down: bathymetry.	14
Figure 7	Velocity field for scenario 01 at different time intervals, after 24, 72 and 120 hours from the initial time.	17
Figure 8	Validation plots. On the left. Box plot of Normalized Root Mean Square Error, Hanna Heinold, Pearson Correlation, Skill coefficient; on the right: Taylor diagram.	19
Figure 9	- Typical output of the atmospheric modelling	22
Figure 10	- Atmospheric output structure	23
Figure 11	- Risk assessment model.	25
Figure 12	- TESEO numerical model domain for Genoa's port area	33
Figure 13	- TESEOsimulation form at PROMPT DSS.....	35
Figure 15	- Example of TESEO's trajectory results in Tripoli port area	37
Figure 16	- Releasing positions for oil (top) and HNS (down) spills.....	39
Figure 17	- Location of the spill points in the Port of Tripoli.	42





Figure 18 - Location of the spill points in the Port of Aqaba45

Figure 19 - ETA and hazard map for the HNS (on the left), and for the Oil (on the right).54

Figure 20 - Physical vulnerability index for water pollution from OIL spills in the Port of Genoa.55

Figure 21 - Environmental vulnerability index for water pollution from OIL/HNS spills in the Port of Genoa.....56

Figure 22 - Pop-up window to launch atmospheric pollution simulation of the evaporated part of the substance.....61

Figure 23 - Example of pollutant concentration between 0 and 10 m over the sea surface at Tripoli (left) and Aqaba (right) port area62

List of tables

Table 1 - Physical parameter of the model.....13

Table 2 - TESEO setup parameters and coefficients for Genoa's port area33

Table 3 - List of available substances for forecast on-demand in PROMPT DSS35

Table 4 – Oil spill points in Genoa.....40

Table 5 – HNS spill points in Genoa.41

Table 6 – Oil spill scenarios selected in the Port of Tripoli.....43

Table 7 – HNS spill scenarios selected in the Port of Tripoli.....44

Table 8 – Oil spill scenarios selected in the Port of Aqaba.46

Table 9 – HNS spill scenarios selected in the Port of Aqaba.47

Table 10 - Physical vulnerability levels.48

Table 11 - Environmental vulnerability levels.....49

Table 12 - Socio-economic vulnerability levels.....49

Table 13 - Human vulnerability levels.....50

Table 14 - Socio-economic vulnerability levels.....50

Table 15 - Hazard levels.51

Table 16 - Risk weights.....51

Table 17 - Standardized risks.52

Table 18 – Risk levels.52





1. INTRODUCTION

Understanding the dispersion and impact of pollutants such as oil and hazardous and noxious substances (HNS) in marine and coastal environments is critical to protecting these ecosystems and mitigating risks to human health, economic activities, and biodiversity. This document outlines a comprehensive approach for modelling both marine and atmospheric dispersions of pollutants, focusing on high-risk areas and providing tools for real-time and forecasted analysis of pollutant transport. The study covers multiple geographic regions where the risk of accidental spills is significant, emphasizing the Gulf of Genoa, Aqaba, and Tripoli as case studies.

Section 1 introduces these study areas, followed by an overview of the methodologies applied in each location, detailing the integration of hydrodynamic and atmospheric models to simulate pollutant dispersion accurately. These models, driven by detailed metocean data, form the basis for simulating pollutant behaviour and are essential for the predictive modelling of spill events.

Section 2 elaborates on the **Metocean Modelling** component, which includes high-resolution impact hydrodynamic and atmospheric models that characterize the physical conditions influencing the spread and persistence of pollutants. These models provide essential inputs for understanding current patterns, wind forces, and other factors that play crucial roles in pollutant transport.

In Section 3, the document delves into **Pollution Modelling**, distinguishing between the behaviour and of oil spills and chemical releases in the marine and atmospheric environments. The TESEO model is described and applied to simulate oil transport, dispersion, and weathering processes, capturing the fate of spills under various environmental conditions. Additionally, HYSPLIT is utilized to forecast the atmospheric transport of toxic substances resulting from chemical spills, facilitating an integrated approach to managing both waterborne and airborne pollutants.

This document also introduces an **On-Demand Forecasting** system that provides rapid-response predictions based on observed spill locations, supported by satellite data and remote sensing for early spill detection. Risk assessment methodologies, outlined in the latter sections, combine hazard analysis, vulnerability assessment, and comprehensive risk mapping to inform stakeholders about potential environmental impacts and guide decision-making in response to pollution events.





By applying advanced modelling frameworks and integrating real-time data sources, this document serves as a technical foundation for understanding and managing the risks associated with accidental pollutant releases in sensitive coastal regions.

1.1. Study Areas

The three study areas planned to focus on this project include the port of Genoa (Italy), the port of Tripoli (Lebanon), and the Gulf of Aqaba (Jordan).

The former sites are located in the Mediterranean Sea and the latest is in the Red Sea. The port of Genoa is located in the Ligurian Sea (Northwestern Mediterranean), latitude $44^{\circ} 4' 03''$ N and longitude $8^{\circ} 86' 2''$ E, is the largest commercial port in the Mediterranean Sea. The computational domain developed for this study covers the Gulf of Genoa, with the external boundary width equal to 80 km, and the distance from the port equal to 20 km (Figure 1).

The port of Tripoli geographically located in the Eastern Mediterranean Sea, Northern area of Tripoli city at $34^{\circ}27'03''$ N $35^{\circ}49'43''$ E is among the most important port on the eastern basin of the Mediterranean Sea since it serves as a link between East and West. Figure 2 shows computational domain used for port of Tripoli. The domain consists of a semicircle area with an arc length of 32 km radius of 9 km and, covering a distance of 5.6 km from the port's maximum protrusion to the open boundary. The Gulf of Aqaba, located at $28^{\circ}45'N$ $34^{\circ}45'E$, is a narrow, deep and long most northern extension of the Red Sea. The gulf is the only access of Jordan to the sea and surrounded by dry desert mountains, no riverine inputs and only a negligible runoff. Computational domain utilized for modelling of Gulf of Aqaba is depicted in Figure 3. The domain covers a long and relatively narrow area with a length of 50 km and a variable width of 5 to 20 km from the northern part of the gulf to the offshore part, respectively.



Figure 1 Plan view of the Genoa harbor's computational domain



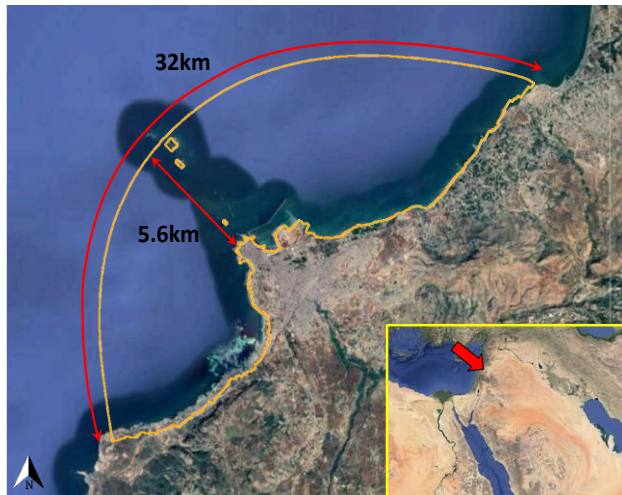


Figure 2 Plan view of the Tripoli harbor's computational domain

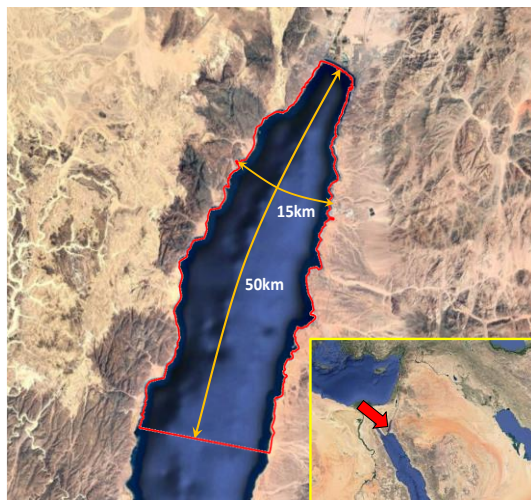


Figure 3 Plan view of the Aqaba harbor's computational domain



1.2. General Methodology

The Prompt system has been developed to be a valuable tool for facing marine pollution emergencies produced by oil and Hazardous and Noxious Substances (HNS) (or chemical) spills. To achieve this objective, the system comprises the following main elements (see Figure 4):

- i) High-resolution metocean data: to provide pollution modelling, it is necessary to know the main variables that dominate the processes of dispersion and evolution of the pollutants. For that reason, it is required to have a high-resolution modelling of the ocean currents and winds at the sites. These results are the first input of the pollutant modelling
- ii) Remote sensing for the identification of oil spills: thanks to remote sensing it is possible to monitor the sea to detect oil slicks even under varying weather conditions and during both day and night. Upon detecting an oil spill, remote sensing data allows operators to rapidly initiate on-demand simulations, utilizing the observed spill location as a starting point to forecast the pollutant's trajectory.
- iii) On-demand forecast modelling: the system provides the ability to model and predict the trajectory of oil and HNS spills and the evolution of the main physicochemical processes of the substance. Moreover, when a chemical substance produces evaporation, the system will analyze the evolution of the pollutant in the atmosphere using a coupling with an atmospheric pollution model. The core of the system is based on the spill numerical model TESEO developed by IHCantabria to simulate the fate, transport and dispersion of oil and chemical spills in the marine environment. TESEO is coupled to an air quality numerical model (HYSPLIT from NOAA) to predict the HNS evolution at the whole marine environment (seawater and atmosphere) (see more details in Section 3). As forcings, the system uses the pre-run metocean scenarios (described in step i) statistically representative of the variability of the study site. As result, the system provides in real time spill trajectories and weathering forecasting (with a maximum temporal horizon of 5 days) of oil and HNS spills in the marine environment as well as the forecasting of the dispersion in the atmosphere of the toxic cloud.
- iv) Oil and HNS Risk assessment system: the system provides the hazard, vulnerability and risk maps, both in the marine environment and in the

Commentato [ASAJ1]: @Mattia, I would suggest to include a paragraph with the main points of the system to highlight the contribution of the main important technical parts (as we have done with the spill modelling part) and mention Figure 4 for the understanding of the complete system. I would suggest something like this:

The Prompt system has been developed to be a valuable tool for facing marine pollution emergencies produced by oil and Hazardous and Noxious Substances (HNS) (or chemical) spills. To achieve this objective, the system comprises the following main elements (see Figure 4):

- i) High-resolution metocean data (including a description paragraph)
- ii) Remote sensing for the identification of oil spills (including a description paragraph)
- iii) On-demand forecast modelling (as described in the document)
- iv) Oil and HNS Risk assessment system (as described in the document)

Commentato [ASAJ2]: @Mattia, please adapt this according to final structure of this part





atmosphere, due to accidental oil and HNS spills. The risk is estimated as the combination of hazard and vulnerability. Hazard is defined as the probability of the environment (marine and atmosphere) to be polluted by an oil/HNS spill. The hazard is calculated on the basis of a high number of numerical simulations that represent the metocean variability of the site (pre-run metocean scenarios mentioned in step i) and the potential spill scenarios. The numerical simulation of the evolution of the pollutant in the marine environment and in the atmosphere is carried out based on the aforementioned coupling between TESEO and HYSPLIT models. The vulnerability assessment integrates physical, biological, and socio-economical aspects as well as the vulnerability to the population. As result, the system provides physical, environmental, socio-economic and risk maps to population, both for marine and atmospheric pollution. The risk assessment system provides valuable results for planning and preventing possible emergencies.

Commentato [ASAJ3]: Same comment

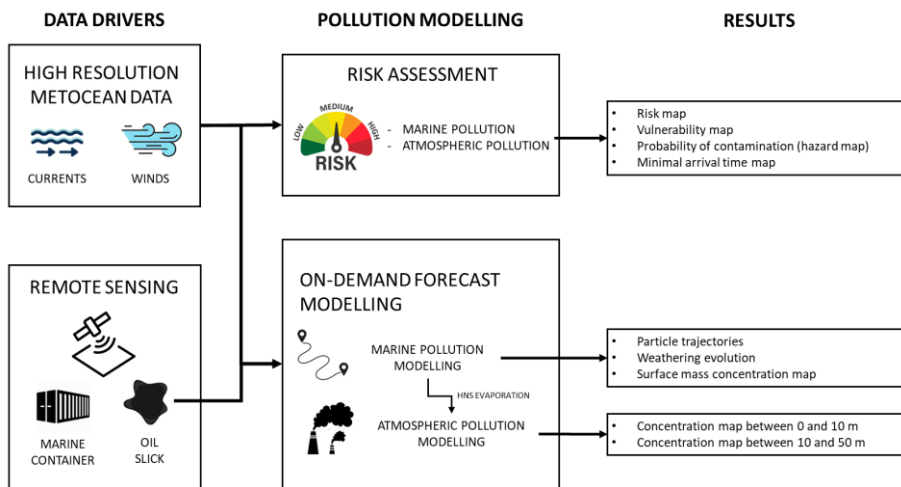


Figure 4 - General framework of the system

PROMPT DSS is the evolution of BeReady DSS. During this project some new implementations of the previous DSS are planned. All the sites and all features of BeReady will remain and a list of new implementations will be added to the new PROMPT system.





Figure 5 shows all the features of the system by site, the features developed during the PROMPT project are marked as “new”.

It is important to mention that in the sites where an upgrade of the meteocean variables is planned, the risk assessment is updated to provide final users with the best quality results possible. Therefore, the risk assessment in the marine environment carried out in Tripoli and Aqaba has been updated in the framework of PROMPT project to update the analysis with the new high-resolution atmospheric data developed in PROMPT.


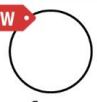

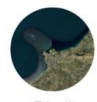
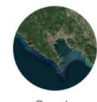




























				
DSS INTEGRATION	 Genoa	 Aqaba	 Tripoli	 Spezia
HIGH-RES FORCINGS	 	 	 	
MODELLING ON DEMAND	 	 	 	
RISK ASSESSMENT (STATISTICAL)	 	 	 	
 REMOTE SENSING	 	 	 	

Figure 5 - Features of the system implemented by site.



2. METOCEAN MODELLING

2.1. Hydrodynamic modelling

The hydrodynamics of the Gulf of Genoa was simulated using the Delft3D 4 numerical model. From both an application and development and research perspective, this numerical model is one of the most robust and trustworthy tools for understanding the dynamics water environments. Delft3D consists of a variety of dynamically interfacing modules for the exchanging of data and results, each addressing a particular domain of interest such as flows, sediment transport, waves, water quality, morphological developments, and ecology. Among the available module embedded in the package, Delft3D-FLOW, the module adopted in this work, is an integrated flow and transport modelling system enabling a multi-disciplinary approach and 3D calculations for the coastal, river, and estuarine regions.

2.1.1. Model description

DELFT3D-FLOW solves the unsteady shallow-water equations in two (depth-averaged) or three dimensions. The system of equations consists of the horizontal momentum equations, the continuity equation, the transport equation, and a turbulence closure model. The model employs Cartesian x-y coordinates for the horizontal plane and applies the so-called “ σ -coordinate transformation” along the vertical direction; this allows mapping the irregular physical domain included between the wavy free surface and the uneven bottom, into a regular computational domain. Under the hypotheses of hydrostatic pressures and incompressible fluid, the momentum balance in the horizontal plane reads:

$$\frac{\partial u}{\partial t} + u \frac{\partial u}{\partial x} + v \frac{\partial u}{\partial y} + \frac{\omega}{h} \frac{\partial u}{\partial \sigma} - f v = -g \frac{\partial \zeta}{\partial x} + \nu_H \left(\frac{\partial^2 u}{\partial x^2} + \frac{\partial^2 u}{\partial y^2} \right) + \frac{1}{h^2} \frac{\partial}{\partial \sigma} \left(\nu_V \frac{\partial u}{\partial \sigma} \right) + M_x \quad (1)$$

$$\frac{\partial v}{\partial t} + u \frac{\partial v}{\partial x} + v \frac{\partial v}{\partial y} + \frac{\omega}{h} \frac{\partial v}{\partial \sigma} - f u = -g \frac{\partial \zeta}{\partial x} + \nu_H \left(\frac{\partial^2 v}{\partial x^2} + \frac{\partial^2 v}{\partial y^2} \right) + \frac{1}{h^2} \frac{\partial}{\partial \sigma} \left(\nu_V \frac{\partial v}{\partial \sigma} \right) + M_y \quad (2)$$

where u , v and ω are the velocity components along x , y and σ respectively, t is time, g is gravity, f is the Coriolis parameter, h is the total water depth and ζ is the free surface elevation above the still water depth, d ($h = d + \zeta$). Note the σ -coordinate is scaled as $\sigma = (z - \zeta)/(2\zeta + d)$, giving $\sigma = -1$ at the bed and $\sigma = 0$ at the free surface. As far as the quantities at the right-hand side of Eqs. (2) and (3) are concerned, ν_H and ν_V represent the horizontal and vertical viscosity coefficients respectively, whereas M_x and M_y are external sources or sinks of momentum, discharge or withdrawal of water. The vertical velocity ω is computed by integrating the continuity equation:





$$\frac{\partial \omega}{\partial \sigma} = -\frac{\partial \zeta}{\partial t} - \frac{\partial [(d+\zeta)u]}{\partial x} - \frac{\partial [(d+\zeta)v]}{\partial y} \quad (3)$$

Kinematic and dynamic boundary conditions

In Delft3D-FLOW, kinematic and dynamic boundary conditions are imposed at the bottom ($\sigma = -1$), free surface ($\sigma = 0$), as well as the lateral boundary of computational domain (; the following equations hold:

$$\omega|_{\sigma=0,-1} = 0 \quad (4)$$

$$V \cdot \nabla l|_{l(x,y)} = 0 \quad (5)$$

Dynamic boundary conditions are imposed at the bed ($\sigma=-1$) and free surface ($\sigma=0$), according to the equation:

$$\left[\frac{v_Y}{d+\zeta} \cdot \frac{\partial u}{\partial \sigma} = \frac{\tau_{\sigma x}}{\rho}; \frac{v_Y}{d+\zeta} \cdot \frac{\partial v}{\partial \sigma} = \frac{\tau_{\sigma y}}{\rho} \right]_{\sigma=0,-1} \quad (6)$$

$$\tau|_{l(x,y)} = 0 \quad (7)$$

in which represents the shear stress at either the bottom or the free surface and is the horizontal velocity vector. It is noteworthy that the Eq. (4b) assumes the grid size to be larger than the thickness of the boundary layers occurring in the flow, which makes it reasonable to set a “no-slip condition” on.

Bottom shear stress

The bottom shear stress, τ_{-1} , is modelled as:

$$\vec{\tau}_{-1} = \frac{\rho g \vec{u}_b |\vec{u}_b|}{C_{3D}^2} \quad (8)$$

where C_{3D} is the 3D-Chezy coefficient and is the velocity just above the bed. A Chezy coefficient equal to $65 \text{ m}^{1/2}/\text{s}$ was used to estimate bed shear stress.

Wind drag

Wind drag on the sea surface can be modeled as:

$$\vec{\tau}_0 = \rho_a C_{D10} U_{10}^2 \quad (9)$$

where ρ_a is the air density, U_{10} is the wind speed 10 m above the sea level, and C_{D10} is a dimensionless drag coefficient.





Numerical solution

Delft3D-FLOW uses a “Cyclic” Finite Difference Method (C-FDM) to solve both the horizontal momentum and continuity equations. As widely discussed in Lesser et al. (2004), C- FDM extends the Alternating Direction Implicit Method (ADIM) introduced by Leendertse (1987), adding a special approach for the horizontal advection terms. The latter consists in splitting the third-order upwind finite-difference scheme for the first derivative, into two second-order consistent discretization, which are then employed in both the stages of ADIM (Stelling and Leendertse, 1991). Physical characteristics utilized for numerical setup are summarized in Table 1.

Table 1 - Physical parameter of the model

physical parameter	
number of sigma layer	11
time step (min)	0.05
Chezy coefficient	65
wind drag coefficient	0.0063
turbulence model	k-ε
horizontal eddy viscosity	0.1
horizontal eddy diffusivity	1
vertical eddy viscosity	1.00E-06
vertical eddy diffusivity	1.00E-06
advection scheme for momentum and transport	cyclic

2.1.2. Model application

Grid and Bathymetry



UCPM-2022-PP/G.A-101101263-PROMPT



An orthogonal regular staggered Arakawa-C grid in a Cartesian co-ordinate system was used for developing Genoa mesh (Figures 7). In such grid, the water level is calculated at the centre of each grid cell and the velocity components (i.e. u and v) are defined perpendicular to the midpoint of side faces of each cell. The mesh counts for 61553 cells, 604 along the M-direction, 178 along the N-direction. The resolution ranges from 50 meters inside the port, to 250 meters offshore.

High bathymetric survey was used to obtain information on seabed topography. Two interpolation methods on computational grid are used to obtain bathymetry. Hence, both grid cell averaging method, for the areas with a high sample density, and triangular interpolation method, for the areas with a low sample density, were applied to create integrated spatially varying depth. Figure 10 shows the water depth across the computational domain, as well as the port's interior portion of the Genoa harbour. It is possible to see the two sub-marine canyons off Genoa coast, which affect the water circulation and the nutrient transport in the Ligurian Sea.

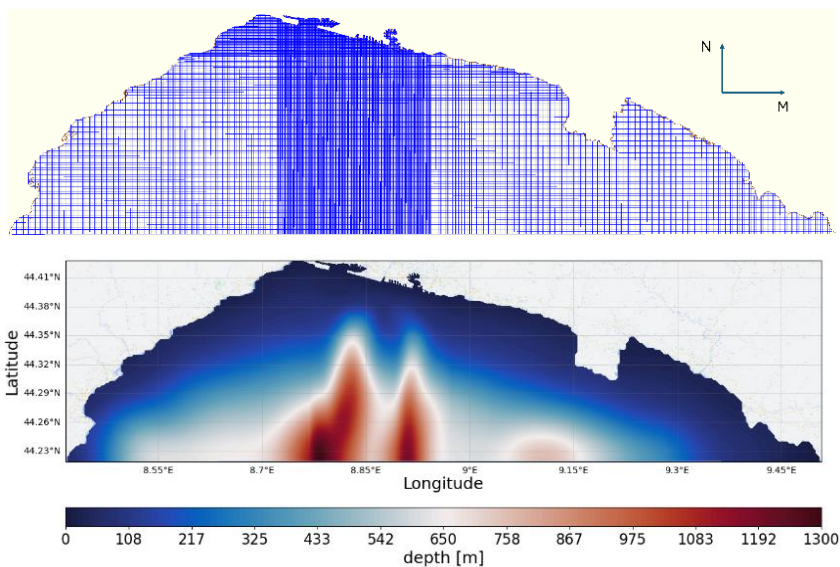


Figure 6 On top: high resolution regular grid; down: bathymetry.





Scenarios selection

To capture the variability in wind and wave conditions for the Gulf of Genoa, we leveraged a comprehensive 40-year hindcast dataset developed by the MeteOcean research group at the University of Genoa (DICCA). This dataset provides hourly wind and wave data across the entire Mediterranean Sea with a spatial resolution of 10 km. Given the vast quantity of data, a systematic method was necessary to extract representative scenarios while retaining key dynamic features of the region.

Our selection process used significant wave height as the primary reference variable. The user defines the desired temporal window, in this case one week, and an algorithm evaluates the dataset week by week, identifying peaks in wave height at the center of each window. If a peak is found, the corresponding week is retained. Otherwise, the algorithm moves forward by one day and reassesses the next week, ensuring that no relevant events are overlooked. This process continues across the entire dataset, resulting in an initial set of weeks characterized by significant wave events.

The selected weeks are further grouped based on four key wave characteristics:

1. **Wave Energy:** The sum of squared wave heights during the week is calculated and normalized between 0 and 1, allowing us to classify weeks by energy level.

$$SPI = \sum_i H_{s_i}^2 \quad (10)$$

Where H_{s_i} represents the significant wave height at time i . Values near 0 indicates low-energy events, values near 1 signifying high-energy events and values around 0.5 medium energy events.

2. **Wind-Wave Relationship:** The second parameter examines the correlation between wind and wave directions. If wave heights rise in response to increasing wind velocity, and their mean directions are close, the two signals are considered correlated, reflecting wind-generated waves. A lack of correlation indicates the presence of swell or random waves not directly driven by local winds.

$$\Delta = \bar{\theta}_{wv} - \bar{\theta}_{wnd} \quad (11)$$

$$\rho = \text{cor}(H_s, U_{wnd}) \quad (12)$$

Where $\bar{\theta}_{wv}$ and $\bar{\theta}_{wnd}$ are the wave and wind directions averaged over the week and U_{wnd} is the wind speed.





3. **Directional Spread:** The standard deviation of wave direction during the week allows to distinguish low-spread events, where waves consistently come from the same direction, from high-spread events, where wave directions vary significantly over the week.

$$\sigma(\theta_{wv}) \quad (12)$$

4. **Wave Direction:** This parameter categorizes the predominant wave direction ($\bar{\theta}_{wv}$) into one of eight possible directional bins.

These parameters allow us to systematically classify the weeks into distinct scenarios. Although the maximum theoretical number of combinations was 96, we identified 23 unique scenarios. From each scenario, we selected the most representative week by calculating the deviation from the mean of all weeks within the cluster. This resulted in a final set of 23 weeks, each characterized by its unique properties, date, and frequency of occurrence.

With this carefully selected set of scenarios, we downloaded large-scale current from the Mediterranean Sea Physics Reanalysis of Copernicus Marine Service and tidal data from TPXO global tidal model, for the corresponding periods, providing the necessary boundary conditions to proceed with the implementation of the 3D hydrodynamic model for pollutant dispersion simulations.





Results

The following figures represent an example of marine circulation in Genoa ports at various time intervals, for scenario 01.

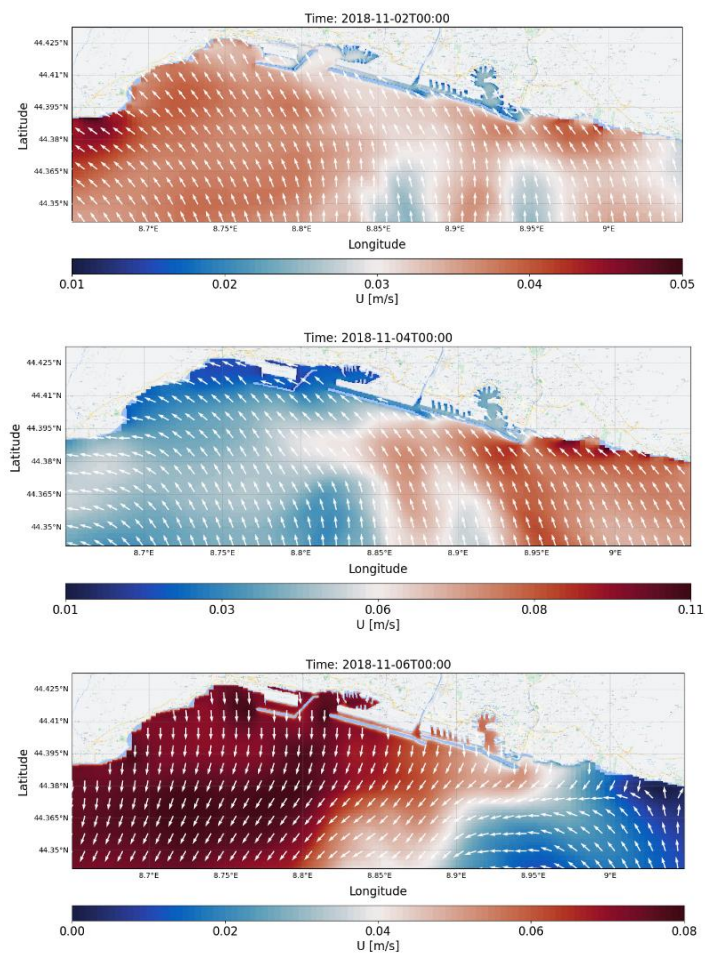


Figure 7 Velocity field for scenario 01 at different time intervals, after 24, 72 and 120 hours from the initial time.



UCPM-2022-PP/G.A-101101263-PROMPT



Model Validation

To assess the realism of the model outputs, water level measurements taken inside the port (at the location marked by the red dot on the map) were used to validate the simulated current scenarios. The validation focused on comparing the model results to observed data through a variety of statistical methods, as shown in the accompanying plots.

On the left side of the figure, box plots summarize four commonly used indices:

1. **Normalized Root Mean Squared Error (NRMSE):** This statistic quantifies the average difference between model predictions and observations, normalized by the range of observed values. An NRMSE closer to zero indicates better model accuracy.
2. **Hanna-Heinold Statistic:** This statistic is another measure of model performance, designed for atmospheric models but applicable in other contexts. It should also tend toward zero when the model is well-calibrated against observations.
3. **Pearson Correlation Coefficient:** This is a measure of the linear relationship between model predictions and observations. A value of 1 indicates perfect correlation, meaning that the model captures the variability of the observed data accurately.
4. **SKILL Score:** This is a composite index that evaluates model performance by combining the correlation and error metrics. A SKILL score of 1 reflects a perfect model, while values close to zero indicate poor performance.

These box plots help visualize the distribution of each statistic across multiple time points or scenarios, highlighting the median, quartiles, and any potential outliers. The general trend shows favorable agreement between the model and the observations, with some outliers that may warrant further investigation.

On the right side, a Taylor diagram provides a more comprehensive comparison between model outputs and observations, using three key statistics:

- **Pearson Correlation:** Reiterated here to show the linear correlation between the model and observations.
- **Root Mean Square Error (RMSE):** Visualized as the radial distance from the origin. Lower RMSE values, closer to the observed data point, indicate better model performance.
- **Standard Deviation:** Represented as the angle around the diagram, this indicates how well the model reproduces the variability seen in the observations.





In the Taylor diagram, the violet circle represents the observed data. Model results are displayed as diamonds, and the closer these diamonds are to the violet circle, the better the model's performance. Finally, the colors of the diamonds are in function of the bias in centimeters. The diagram confirms that the model performs quite well in reproducing the observed water levels, especially considering the complexity of the Gulf of Genoa's coastline and the numerous environmental variables influencing the currents.

Overall, the validation indicates that the model provides reliable simulations, although further investigation of the outliers may help refine the results even more.

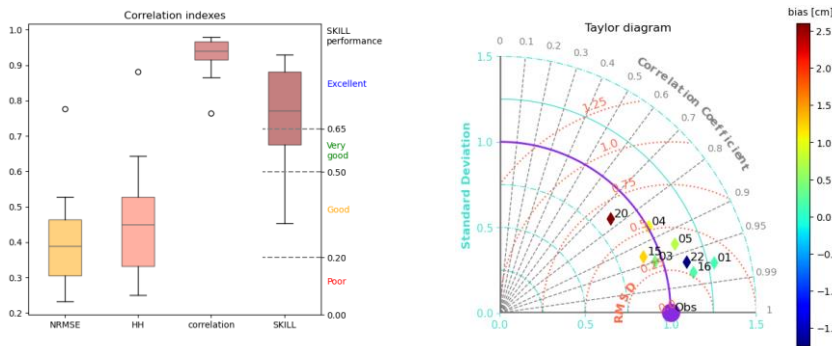


Figure 8 Validation plots. On the left: Box plot of Normalized Root Mean Square Error, Hanna Heinold, Pearson Correlation, Skill coefficient; on the right: Taylor diagram.

2.2. Atmospheric modelling

A state-of-the-art modelling chain was established using the Weather Research and Forecasting (WRF) model. WRF is a non-hydrostatic numerical model designed for both research and operational applications, developed collaboratively by institutions including NCAR, NOAA, and NCEP. It is renowned for its flexibility and accuracy, making it ideal for high-resolution simulations.

2.2.1. Model description

2.2.2. Model description

The Weather Research and Forecasting (WRF) model is a cutting-edge, next-generation numerical weather prediction system designed for both atmospheric research and operational forecasting. The Advanced Research WRF (ARW) core is one of the two primary





dynamical cores within the WRF system, the other being the Nonhydrostatic Mesoscale Model (NMM). Developed collaboratively by the National Center for Atmospheric Research (NCAR), the National Oceanic and Atmospheric Administration (NOAA), and other leading institutions, WRF-ARW has become one of the most widely used atmospheric models in the scientific community. Its robust design, flexibility, and precision make it an invaluable tool for simulating weather, climate, and atmospheric dynamics on a wide range of scales.

Model Characteristics

The WRF-ARW core is a non-hydrostatic, fully compressible atmospheric model. Its primary objective is to provide high-resolution simulations of atmospheric phenomena, capable of resolving features from global scales down to small, localized weather systems like thunderstorms. The model's non-hydrostatic formulation allows it to accurately simulate vertical motion, which is essential for capturing convective processes such as thunderstorms and orographic lifting.

Key characteristics of the WRF-ARW model include:

1. **Non-hydrostatic Dynamics:** This allows WRF-ARW to model small-scale processes that involve vertical motion, like convection, without making the hydrostatic approximation. This is crucial for capturing fine-scale phenomena.
2. **Fully Compressible Equations:** The model solves the full set of primitive equations of motion for the atmosphere, which allows it to simulate phenomena with high precision in both space and time.
3. **Nested Domains:** WRF-ARW supports the use of nested grids, which means users can run simulations with varying levels of resolution within the same model run. This feature allows for high-resolution domains nested within lower-resolution global models, making it ideal for both regional and local-scale studies.
4. **Customization and Modularity:** WRF-ARW is highly modular, allowing users to select different physics schemes for microphysics, planetary boundary layer (PBL), radiation, and surface physics. This flexibility ensures that users can tailor the model to their specific research or operational needs.

Physics Option

WRF-ARW offers a variety of physics parameterization schemes that can be adjusted depending on the specific application or research focus. These physics options include:



UCPM-2022-PP/G.A-101101263-PROMPT



1. **Microphysics:** Microphysics schemes are critical for simulating clouds, precipitation, and related processes. WRF-ARW provides a range of microphysics options, from simple schemes that focus on bulk properties to more sophisticated ones that simulate the interaction of different cloud hydrometeors, such as cloud water, ice, snow, and graupel.
2. **Planetary Boundary Layer (PBL):** The PBL parameterization represents the turbulent processes that occur in the lowest part of the atmosphere, influencing surface-atmosphere interactions. WRF-ARW supports multiple PBL schemes, including the Yonsei University (YSU) scheme and the Mellor-Yamada-Janjic (MYJ) scheme, which are commonly used in atmospheric research and forecasting.
3. **Cumulus Parameterization:** Although WRF-ARW is often run at resolutions where convection can be explicitly resolved (e.g., less than 4 km grid spacing), cumulus parameterization schemes are still used for larger-scale simulations. These schemes approximate the effect of sub-grid scale convective processes.
4. **Radiation:** The WRF-ARW model includes longwave and shortwave radiation schemes that account for the interaction of radiation with gases, aerosols, and clouds. These radiation schemes are important for determining surface energy budgets and driving atmospheric circulation.

Land-Surface Models (LSMs): The LSMs represent surface-atmosphere exchanges of heat, moisture, and momentum. WRF-ARW can use a variety of LSMs, such as the Noah model, which is widely employed for operational weather forecasting.

Numerical Methods and Grid Structure

WRF-ARW employs advanced numerical methods to solve the atmospheric equations, ensuring high accuracy and computational efficiency. It uses a terrain-following hydrostatic pressure (eta) coordinate system, which allows the model to better represent mountainous terrain and steep gradients in topography. The grid structure is Arakawa-C, which ensures a more accurate representation of physical processes, especially for wind and pressure interactions.

One of the key innovations in WRF-ARW is the ability to utilize adaptive time stepping and advanced interpolation techniques, allowing for enhanced computational speed without sacrificing accuracy. Additionally, the Runge-Kutta time integration scheme used in WRF-ARW offers stability in numerical computations, making it possible to run long-term simulations or high-resolution simulations with a fine temporal resolution.





2.2.3. Model application

Two specific domains were defined for the regions of Aqaba and Tripoli. These domains were selected based on the project's requirements to capture localized atmospheric conditions with high precision. For this purpose, high-resolution fields with a horizontal resolution of 1.1 km x 1.1 km were defined.

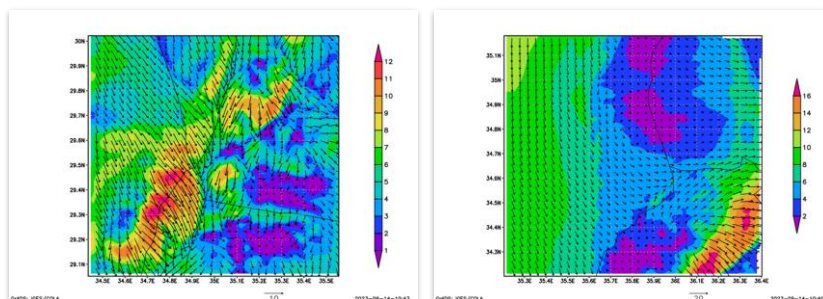


Figure 9 - Typical output of the atmospheric modelling

The downscaling of global weather forecast models to these high-resolution domains was achieved using a one-way nesting procedure, which allows for the integration of coarse global data into finer local domains. The nesting procedure was essential for refining large-scale meteorological data to capture the variability and detail required for local climate simulations.

Scenarios Selection and Simulation

The atmospheric simulations were carried out for a subset of possible scenarios, carefully chosen to represent the variability of the local climate. These scenarios were selected using big data analysis algorithms, which identified key time frames that needed to be downscaled. This strategic approach ensured that the simulations covered the range of atmospheric conditions that could influence pollutant behavior in the target regions. The WRF model was configured to run high-resolution simulations over these selected time frames, providing the necessary meteorological data for subsequent pollutant dispersion analysis.

Post-processing and Data Transformation

Following the atmospheric simulations, an intensive postprocessing phase was conducted to prepare the WRF model outputs for integration with the TESEO platform, which





is the core of PROMPT DSS system. This phase involved several key steps to ensure that the data met the platform’s specific requirements.

The WRF model outputs originally consisted of an ensemble of 2D to 10D matrices representing 117 different parameters. Each file contained one hour of meteorological data. However, only five of these parameters were considered relevant to the project objectives and the TESEO platform. These key parameters, including wind speed, temperature, and humidity, were extracted and used to create the final output files. To meet the platform’s requirements, the data were transformed from the WRF’s native X-Y grid to a smaller latitude-longitude grid. This process involved reparametrizing the grid and applying interpolation techniques to reconcile any discrepancies between grid points.

The WRF outputs, initially available as hourly data files, were merged into a total of 50 final files, 25 for each region (Aqaba and Tripoli). Each file was structured to represent distinct atmospheric scenarios, as defined in the earlier stages of the project. For each location and scenario, 168 individual 2D fields were merged into 3D matrices, ensuring that the data were correctly aligned within the desired coordinate system and limited to the specific areas of interest. This approach allowed the project team to generate a compact, high-resolution dataset, tailored for integration with the TESEO platform for further analysis and visualization.

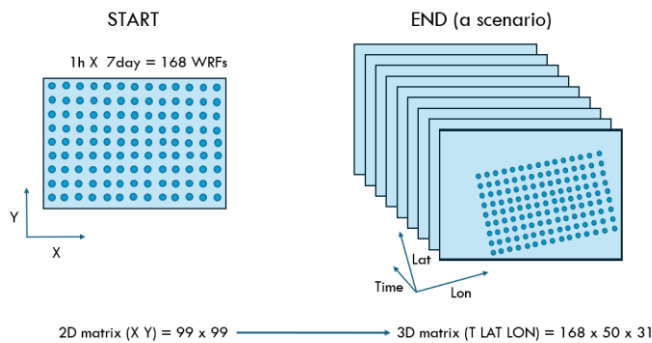


Figure 10 – Atmospheric output structure





3. POLLUTION MODELLING: OIL AND CHEMICAL SPILLS

3.1. General framework for pollution risk assessment

One of the objectives of PROMPT is to develop a Risk Assessment Model for oil spills in marine environments and for HNS spills in marine and atmospheric environments. The Risk Assessment Model will support the response planning, providing the hazard, vulnerability and risk of the environment to oil and HNS spills in terms of probability. In other words, the risk assessment system will help planes and decision-makers answer many important planning questions such as:

Where may take place the potential spills?

What are the most likely places to be affected by a spill?

How long will a spill to reach a location?

What areas have to be protection priorities?

As previously mentioned, risk is assumed to be made of hazard and vulnerability (i.e. Risk = Hazard x Vulnerability). Hazard is defined as the probability of the coast and the marine/atmospheric environments (in particular, sensitive areas) to be polluted by an oil or HNS spill and is calculated in probabilistic terms. On the other hand, vulnerability is the environment's ability to cope with, resist and recover from the impact of pollution. Therefore, in order to develop a risk assessment model, both hazard and vulnerability has to be determined for oil in marine environment and for HNS spills in marine and atmospheric environments.

Figure 11 shows a general overview of the risk assessment model. The main steps of the methodology proposed are as follows:

- 1) **Hazard analysis for oil and HNS spills.** The hazard analysis is based on the following steps: i) selection of N oil and HNS spill scenarios (e.g. type of substance, spill point, spill release volume) according to the uses and activities in the different pilot sites; ii) selection of M met-ocean scenarios statistically representative of the pilot sites and obtained according to the methodology described in section 2; iii) numerical modelling ($M \times N$ simulations) of the spill evolution in the marine environment using the aforementioned TESEO model and in the atmosphere using the coupling between TESEO and HYSPLIT models; iv) statistical analysis of the results to obtain the probability maps of pollution and the arrival time of the pollutant to the potential affected areas.





2) **Vulnerability assessment for oil and HNS spills.** The methodology developed in Be-Ready is applied for marine pollution and adapted for atmospheric pollution. Both methodologies integrate different indexes considering the main physical, biological and/or socio-economical characteristics, as well as the characteristics of the pollutants. As a result, vulnerability maps for the different indexes will be defined for oil spills in marine environments and HNS spills in marine and atmospheric environments.

3) **Risk Assessment for oil and HNS spills.** The hazard and vulnerability previously obtained are integrated to assess the risk from spills. As a result, the system provides: i) physical environmental and socioeconomic risk maps for the marine pollution caused by oil spills and ii) human, environmental and socioeconomic risk maps for the marine and atmospheric pollution caused by HNS spills.

The outputs will be available within the Decision Support System (DSS) platform.

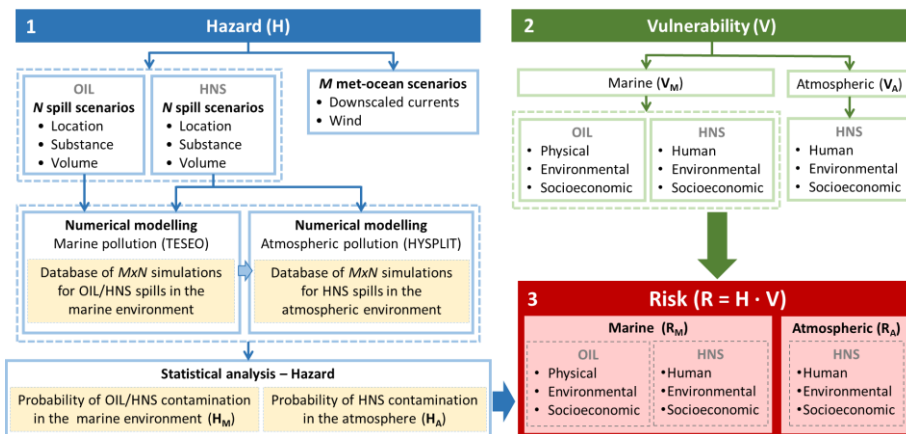


Figure 11 - Risk assessment model.

3.2. Marine pollution modelling

Marine pollution modelling is calculated using TESEO numerical model developed by IHCantabria. This is a Lagrangian numerical model able to calculate the trajectories of a substance released at the sea and its weathering evolution.





During the project, a new site, Genoa has been implemented as a new site to provide oil and chemical modelling. While the sites of Aqaba, Tripoli and La Spezia are preserved on the system from the previous project Be-Ready and will remain fully functional as presented on Figure 5.

3.2.1. Model description (TESEO)

The spill forecast system is based on the state-of-the-art oil spill model called TESEO, developed by the Environmental Hydraulics Institute (IHCantabria) in the framework of several Spanish and European projects (Abascal et al., 2007; Abascal et al., 2017a; Chiri et al., 2020). The HNS forecast module is based on an adaptation of the model for chemical substances, carried out in the framework of SICMA project (<https://sicma.ihcantabria.es/en/>). The Be-Ready operational forecast system integrates both, oil and HNS spill numerical models in a unified version of the model for rapid response in case of accidental pollution.

Therefore, TESEO is a 3D numerical model to simulate the transport, weathering and spatial distribution of oil and HNS spills in the marine environment both at regional scale (offshore) and coastal scale (bays, estuaries and harbours). To achieve this objective the model consists of transport and a weathering module to represent the evolution of the spills in the marine environment. The transport module simulates the drift process of the spilled pollutant by tracking independent numerical particles equivalent to the slick. The evolution of the particles is computed by the superposition of the transport induced by wind, currents and/or waves and turbulent dispersion. The weathering module incorporates the spreading, evaporation, emulsification, dissolution, viscosity and density changes, dispersion in water column, sedimentation and adhesion to coast. TESEO has been calibrated and validated in several studies with drifters buoys (e.g. Sotillo et al., 2008; Abascal et al., 2017a,b).

3.2.1.1. Transport and Dispersion

The transport module of TESEO is based on a Lagrangian approach in which the drift process of the spilled pollutant is described by tracking numerical particles that represents the spill. The spill motion is computed by means of the transport induced by surface currents, wind and/or wave fields, and turbulent diffusion.

The numerical model solves the following vector equation:

$$\frac{dx_i}{dt} = U_a(x_i, t) + U_d(x_i, t) \quad (13)$$





where x_i is the particle position, and U_a and U_d are the advective and diffusive velocities respectively in x_i . For the implementation in the pilot sites, the advective velocity, U_a , is calculated as the linear combination of currents and wind velocity provided by the Met-ocean forecast system described in section 2.

The turbulent diffusive velocity is obtained using a Monte Carlo sampling in the range of velocities and it is assumed proportional to the diffusion coefficient (Hunter et al., 1993).

The velocity fluctuation in each time step is defined as:

$$|U_d| = \sqrt{\frac{6D}{\Delta t}} \quad (14)$$

where D is the diffusive coefficient, in the range 1-100 m²/s (ASCE, 1996).

Besides the turbulent diffusive velocity, the model also incorporates the horizontal expansion of the slick due to mechanical forces such as gravity, inertia, viscous, and interfacial tension, this process is known as oil spreading.

For oil spills, spreading is modelled following Fay (1971). In this process, Fay distinguishes three phases, each of which is determined by dominant spreading and retarding forces on the slick: phase 1, gravity-inertial, which is dominant in the first hour; phase 2, gravity-viscous, which is important from 1 hour to 2 days and phase 3, surface tension-viscous, which is important after 2 days. Using the assumptions adopted by previous researchers (Sebastiao et al., 1995; Berry et al., 2012), the spreading is calculated when the end of phase 1 has been reached according to the following equations:

$$A_0 = \pi \frac{k_2^4}{k_1^4} \left(\frac{V_0^5 g \Delta \rho}{u_w^2} \right)^{1/6} \quad (15)$$

$$A_t = \pi k_2^2 \left(\frac{V_0^2 g \Delta \rho t^{3/2}}{\sqrt{u_w}} \right)^{1/3} \quad (16)$$

where A_0 is the initial area of the surface slick (m²), A_t is the temporal evolution of the area, V_0 is the initial volume of the spill (m³), k_1 and k_2 are empirical coefficients (1.14 and 1.45, respectively according to Berry et al., 2012), ν_w is the kinematic viscosity of water (m²/s),





g is gravitational acceleration (m/s), and $\Delta\rho$ is the relative difference between water density and oil density given by:

$$\Delta\rho = \frac{\rho_w - \rho_o}{\rho_w} \quad (17)$$

where ρ_w is the density of water and ρ_o is the density of oil (kg/m³).

For HNS spills the spreading is calculated based on Kolluru (1992) and Fernandes (2014):

$$\frac{dA_p}{dt} = K_1 A_p^{1/3} + \left(\frac{V_p}{A_p}\right)^{4/3} \left(\frac{A_p}{A_t}\right)^{2/3} \quad (18)$$

where A_p is the area of the individual particle (m²), A_t is the total area of the slick (m²), k_1 is the spreading rate constant (s⁻¹) set to 5787.037 s⁻¹ and V_p is the volume of chemical in individual particle (m³).

3.2.1.2. Weathering processes for Oil spills

Evaporation

Evaporation is usually the most important weathering process for oil spills. It has the greatest effect on the amount of oil remaining on water or land after a spill. In a few days, light crudes can evaporate as much as 75% of the starting oil mass and medium crudes up to 40%. Heavy or residual oils may only evaporate up to 10% of its original mass in the first few days following a spill (ASCE, 1996).

In the present model, the oil evaporation is calculated based on an analytical model proposed by Stiver and MacKay (1984). In their formulation, the rate of evaporation is related to vapour pressure, spill area, a mass transference coefficient that depends on wind speed, environmental temperature, and oil type.

The fraction of oil evaporated is simulated by means of a first order kinetics law as follows:

$$\Delta F = \exp\left[A - \frac{B}{T}(T_0 + T_G F)\right] \left(\frac{k}{e} \Delta t\right) \quad (19)$$

where F is the evaporated fraction, k is the coefficient of mass transfer (which is dependent on the wind speed), A and B are empirical coefficients (6.3 and 10.3, respectively





according to Stiver and Mackay, 1984), e is the thickness of the slick (m), T is the environmental temperature ($^{\circ}\text{K}$), and T_0 and T_G are distillation constants.

The mass transfer coefficient function of wind is expressed as (Lehr, 2001):

$$k = dW^a \quad (20)$$

where a and d are empirical coefficients. The value in the model for them is 0.78 and $2.5\text{E-}3$ respectively, according with the values given by the state of the art (Stiver and Mackay, 1984; Comerma, 2004). W is the wind speed (m/s) at 10 m reference height above the water surface.

Emulsification

Emulsification is the process of the formation of a water-in-oil emulsion increasing the amount of product on the water. The formulation for the formation of water-in-oil emulsions in the TESEO code is based on the work of Mackay et al. (1980) highly used in oil spill numerical modelling (e.g. Rasmussen, 1985; Reed et al., 1989; NOAA, 1994; Comerma, 2004). In this method, the rate of water incorporation is related to wind speed, maximum water-in-oil content, and a constant rate that depends on the type of oil.

Mackay et al. (1980) suggested the following equation to model water uptake:

$$\frac{dY}{dt} = k_{em}(W_{10} + 1)^2 \left(1 - \frac{Y}{Y_{max}}\right) \quad (21)$$

where Y is the water content, Y_{max} is the maximum water-in-oil content, W_{10} is the wind velocity at a height of 10 m over the sea surface, and k_{em} is a constant rate that depends on the oil type. In the model, the constant is equal to $2\text{E-}6$, according with the value given by the state of the art: $k_{em} = [1\text{E-}6\text{--}5\text{E-}6]$ (Rasmussen, 1985; NOAA, 1994; Comerma, 2004).

Physicochemical properties

The physical and chemical properties of the oil change because of weathering processes. In the model, the change in oil density and viscosity over time is related to three different processes: changing water temperature, evaporation, and emulsification. The formulation used to calculate the density and viscosity transformation is described in Comerma (2004).

The total **change in viscosity** of the oil can be expressed as (Mackay et al., 1983):





$$v = v_0 \exp\left(C_T \left(\frac{1}{T} - \frac{1}{T_0}\right)\right) \exp(C_E F) \exp\left(\frac{C_V Y}{1 - C_M Y}\right) \quad (22)$$

where v is viscosity of oil (cSt) for given water temperature, T (°K) (assumed equal to the water temperature), v_0 is the reference viscosity of oil at reference temperature T_0 (°K), C_T , C_E , C_V and C_M are adjusting parameters. In the model, their value are: 0.05, 5, 2.5, and 0.65 respectively, according with the values given by the state of the art: $C_V = [2-3.5]$; $C_M = [0.65-0.654]$; $C_T = [0.018-0.4]$; $C_E = [2-20]$ (Comerma, 2004).

The total **change in density** of the oil can be expressed as (Buchannan and Hurford, 1988):

$$\rho = Y\rho_w + \rho_o(1 - Y)(1 + C_{DE}F)(1 - C_{DT}(T - T_0)) \quad (23)$$

where Y is the water content of the emulsion, ρ_w is the density of water (kg/m^3), ρ_o is the density of initial oil (kg/m^3) at T_o , T_o is the reference oil temperature (°K), T is the environmental temperature (°K), C_{DE} is an empirical constant equal to 0.18 (NOAA, 1994), F is the fraction of oil evaporated from the slick, C_{DT} is an empirical constant equal to $8E-4$ (NOAA, 1994).

3.2.1.3. Weathering processes for HNS spills

Evaporation

The approach followed in TESEO is based on Kawamura and Mackay (1985) and Fernandes (2014). According to these authors, evaporation is estimated based on the following equation:

$$E = A k_n + \frac{M_w P_v}{R T} \quad (24)$$

where E is the evaporation rate (in kg/s), A is the area of the evaporating puddle (m^2), K_m is the mass transfer coefficient (m/s), M_w is the molecular weight of the selected chemical (kg/kmol), P_v is the vapour pressure (in Pa), R is the gas constant ($8314 \text{ J}/(\text{kmol K})$) and T is the air temperature (°K).

The mass transfer coefficient (K_m) can be expressed as Mackay and Matsugu (1973):

$$k_m = 0.0292 U^{7/9} Z^{-1/9} S_c^{-2/3} \quad (25)$$





where U is the wind speed at a height of 10 m (m/s), Z is the pool diameter in the along-wind direction (m) and S_c = the laminar Schmidt number for the selected chemical.

The Schmidt number is a dimensionless number defined as the ratio of the kinematic viscosity and mass diffusivity:

$$S_c = \frac{\nu}{D_m} \quad (26)$$

where ν is the kinematic viscosity of the air, assumed to be $1.5 \times 10^{-5} \text{ m}^2/\text{s}$, and D_m is the molecular diffusivity of the selected chemical in air (m^2/s).

Graham's Law is used to approximate D_m (Thibodeaux, 1979) as:

$$D_m = D_{H_2O} \left(\frac{M_{W(H_2O)}}{M_{W(chem)}} \right)^{1/2} \quad (27)$$

where D_{H_2O} is the molecular diffusivity of water ($2.4 \times 10^{-5} \text{ m}^2/\text{s}$ at 8°C), $M_{W(H_2O)}$ is the molecular weight of water (18 kg/kmol) and $M_{W(chem)}$ is the molecular weight of the selected chemical (kg/kmol).

Correction for volatilization

A volatile chemical is one that has a relatively high vapour pressure at environmental temperatures and therefore evaporates readily. A correction method in the evaporation equation (based in Brighton 1985, 1990; Reynolds 1992) is appropriate only for a chemical at a temperature below its boiling point, as shown below.

$$C = -\frac{P_a}{P_v} \ln \left(1 - \frac{P_a}{P_v} \right) \quad (28)$$

where P_a is the atmospheric pressure (Pa) (101,325 Pa at sea level) and P_v is the vapour pressure of the solute (Pa). For chemicals that are not very volatile, the value of C will be about 1.0. It will increase in magnitude as the vapour pressure of the chemical increases.

The corrected evaporation rate (E_c) is calculated as:

$$E_c = C E \quad (29)$$

where E_c is the evaporation rate corrected for volatility (kg/s).

Dissolution

Dissolution is calculated according to Mackay and Leinonen (1977) and Fernandes (2014). Based on these authors, dissolved mass (Kg) in a specific time period (s) can be represented as follows:





$$M_D = K_d A_s (S \times 10^{-3}) \Delta t \quad (30)$$

where M_D is the dissolved mass (kg), t is time (s), K_d is the dissolution mass transfer (m/s), S is the solubility in water (mg/L), and A_s is the surface area (m²). For the dissolved mass from the surface slick, the surface area of a flat plate is considered.

Mass transfer coefficient can be represented as:

$$K_d = Sh D_i 10^{-4} / L \quad (31)$$

where Sh is the Sherwood Number, D_i is the diffusivity (cm²/s), and L is the characteristic length (m).

The diffusivity (cm²/s) is computed based on Hayduk and Laudie (1974):

$$D_i = \frac{13.36 \cdot 10^{-5}}{\mu^{1.14} V_b^{0.589}} \quad (32)$$

where μ is the water dynamic viscosity (cP) and V_b is the Le Bas molar volume (cm³/mol). This molar volume is obtained as following:

- If chemical is organic: $V_b = 4.9807 M_W^{0.651}$
- If chemical is not organic: $V_b = 2.8047 M_W^{0.6963}$

where M_w is the molecular weight of the chemical (g/mol).

In the dissolution from the surface slick the following formulations are used:

- Surface Area (A_s) is the area of the surface particle (m²)

- Characteristic length: $L = \sqrt{\frac{4 A_s}{\pi}}$

- Sherwood Number: $S_h = 0.578 Sc^{1/3} Re^{1/2}$

where Sc is the Schmidt Number, and Re is Reynolds Number:

- $Sc = \frac{\nu}{D_i}$

- $Re = \frac{V \cdot L}{\nu \cdot 10^{-4}}$

V means the mean velocity of the fluid (m/s); in the case of the surface slick, V is the wind velocity and ν is the water kinematic viscosity (cSt).





3.2.2. Model implementation in Genoa

The Genoa domain has been implemented to perform TESEO simulations of oil and HNS substances at the port area. The domain extension covers the following coordinates:

- Longitude: (8.65°, 9.00°)
- Latitude: (44.35°, 44.43°)

The data used to implement the domain is the bathymetry and the coastline of the area that has been obtained from:

- Bathymetry: obtained and post-processed from the hydrodynamic modelling (section 2.1)
- Coastline: Open Street Maps ([Land polygons](#)) at Mean high water springs (MHWS)

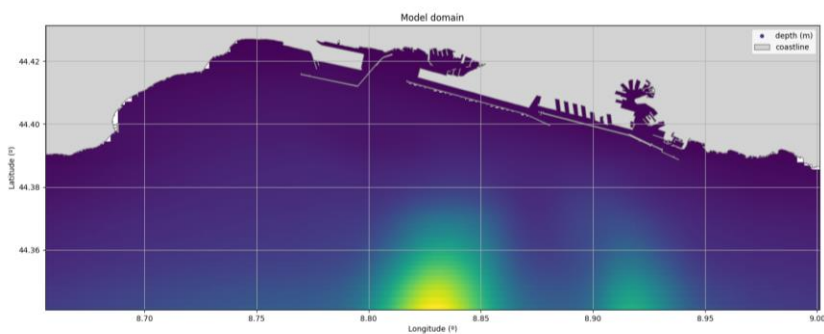


Figure 12 - TESEO numerical model domain for Genoa's port area

Numerical model parameters and coefficients used for the Lagrangian simulations have been summarized in the following table:

Table 2 - TESEO setup parameters and coefficients for Genoa's port area

Variable	Oil simulation		HNS simulation	
	Forecast on-demand	Risk assessment	Forecast on-demand	Risk assessment
Simulation time step (dt)	60 s	60 s	60 s	60 s
Simulation duration	user-defined	72 h	user-defined	72 h
Wind drag coefficient (Cd)	0.02	0.02	0.02	0.02
Turbulent diffusion coefficient (D)	2 m ² /s	2 m ² /s	2 m ² /s	2 m ² /s





Results time step	user-defined	0.5 h	user-defined	
Number of particles	1000	1000	1000	1000
Spreading algorithm	Fay	Fay	Kolluru	Kolluru
Water temperature	user-defined	17°C	user-defined	17°C
Water density	user-defined	1025 kg/m ³	user-defined	1025 kg/m ³
Water kinematic viscosity	1.004e-06	1.004e-06	1.004e-06	1.004e-06
Air temperature	user-defined	15.5°	user-defined	15.5°

3.2.3. On-demand forecast modelling

Forecast on-demand modelling is aligned with the existent methodology used for the rest of the sites implemented during the Be-Ready project. This methodology consists of:

a. Metocean input data (currents and winds) are obtained from the database prepared by UNIGE. This database consists of a group of metocean scenarios (clusters) that describe more than 80% of the metocean variability of each site. Each day UNIGE analyses statistically which are the most plausible scenarios based on regional forecasts and ranked them in the application. This process is done for winds and currents every day. The database provides surface ocean current fields and wind fields at 10m over the sea surface. These variables are the main input to calculate the advection of the substance at the sea surface and the evolution of the weathering conditions (evaporation, emulsion, dissolution...)

b. The user can set up the simulation through the DSS website. The parameters required to be defined by the user are the following:





Location of the release (longitude, latitude)
 Substance to be released
 Volume released
 Date and time of the release
 Duration of the simulation (maximum 5 days)
 Metocean cluster (commented in point a.)
 Water temperature
 Air temperature
 Water density
 Result time step

[New simulation](#) [Show simulation](#)

[Oil](#) [HNS](#)

Longitude: Latitude:

Substances: Volume (m³):

Simulation day: Simulation hour:

Hours of duration: Cluster:

Water temperature (°C): Air temperature (°C):

Density (kg/m³): Result time step:

Figure 13 - TESEOsimulation form at PROMPT DSS

Substances available for on-demand forecast simulations are listed on Table 3.

Table 3 - List of available substances for forecast on-demand in PROMPT DSS

Substance name	
Oil	HNS
FUEL OIL N1-KEROSENO	CRUDE SOY OIL
AUTOMOTIVE GASOLINE	ACETONE
AVIATION GASOLINE 80	ACETIC ACID
BELIDA	ALFAMETHYLSTYRENE
BEKOK	BENZENE
FUEL OIL N1-DIESEL	BUTANE
BRENT BLEND	CYCLOHEXANE
ARABIAN EXTRA LIGHT	CUMENE
FORTIES BLEND	ETHANOL
FUEL OIL N2-DIESEL	ETBE
ARABIAN LIGHT	PHENOL
PRUDHOE BAY	GLYCERIN
TIA JUANA	METHANOL





FUEL OIL N6	METAXYLENE
LAGUNILLAS	MONETHYLENE GLYCOL
	MTBE
	ORTHOXYLENE
	PARAXYLENE
	PROPANE
	PROPYLENE
	CAUSTIC SODA 50%

c. The user triggers the simulation by pressing the “Run simulation” button on the website. This launches a process in the IHCantabria server where the DSS system is hosted and runs the TESEO model on the fly (preprocess all the inputs, run the numerical model, postprocess and publish the results to be managed by the website) Once the simulation is completed the user is redirected directly to the results page to be able to visualize and explore the results.

Results provided from the TESEO simulation are:

- Trajectory of the particles
- Surface concentration results
- Weathering evolution chart

In Aqaba and Tripoli sites, the modelling of atmospheric pollution derived from the evaporation of chemicals is implemented. In these sites, when the marine pollution simulation ends and the substance simulated can evaporate, a pop-up window will ask the user to allow the execution of the atmospheric pollution model.



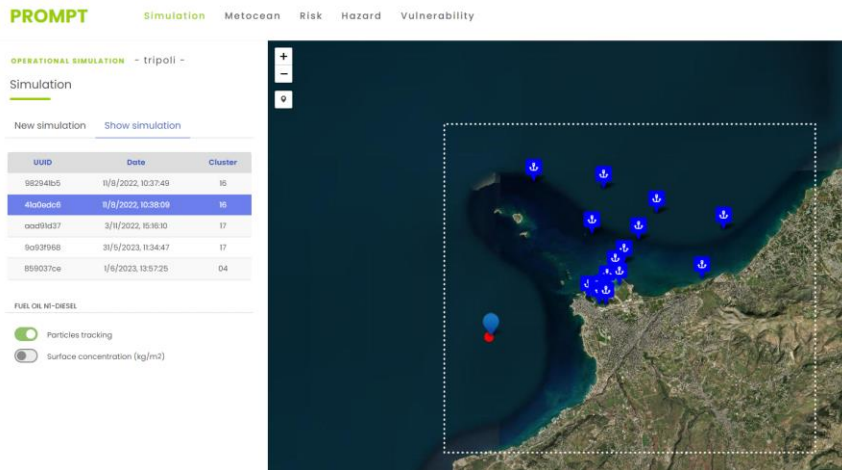


Figure 14 - Example of TESEO's trajectory results in Tripoli port area

3.2.4. Risk assessment methodology

The proposed methodology (see Figure 11) allows to determine the risk in the marine environment and the coastal area affected by an oil or HNS spill based on the work of Galt and Payton (1999), Barker and Galt (2000), Abascal et al. (2010) and Abascal et al. (2015). In this study, the risk is evaluated according to the following expression:

$$R = H \cdot V \quad (33)$$

where R (risk) is the damage or expected losses on the marine environment as a result of an oil or HNS spill at sea; H (hazard) is the probability of a specific coastal or marine area will be affected by the spill and V (vulnerability) is the ability of the environment, to cope, resist and recover from the impact produced by an oil or HNS spill at sea.

Since the definition and implementation of the risk assessment methodology is still in progress, the following sections provide the methods and expected results, as well as preliminary results in some of the study sites.





3.2.4.1. Hazard

As previously mentioned, hazard refers to the probability of a point of being polluted by an oil or HNS spill. The study of the hazard is carried out by the statistical analysis of a hypothetical oil and HNS spill database generated following the following steps:

a) Selection of met-ocean scenarios representative of the study area

As described in section 2, the met-ocean conditions are selected based on the application of classification techniques and dynamical downscaling to obtain high-resolution currents in the pilot sites.

A total of 23, 25 and 25 metocean scenarios has been considered for the Port of Genoa (described in section 2), Aqaba (obtained in Be-Ready project) and Tripoli (obtained in Be-Ready project), respectively.

b) Selection of the spill scenarios

The number of spill scenarios for oil (N_{SC-OIL}) and HNS (N_{SC-HNS}) is estimated based on the following steps: i) selection of the critical points or potential spill locations (N_P); ii) selection of oil products/chemical substances representative of each critical point (N_S) and iii) selection of representative spill volumes (N_V):

$$N_{SC-OIL} = N_P \times N_S \times N_V$$

$$N_{SC-HNS} = N_P \times N_S \times N_V$$

The oil and HNS spill scenarios for each pilot site are presented below:

Port of Genoa (new implementation in PROMPT project)

The Figure 15 **Errore. L'origine riferimento non è stata trovata.** shows the oil spill positions selected (top panel), which reflect the areas of the port most affected by ship traffic, and the HNS spill positions selected (down panel), corresponding to the two docks where the chemicals deposit are located.

A total of 12 oil spill and 13 HNS spill scenarios has been selected (combination of the aforementioned locations, products and volume), as described in Table 4 and Table 5, respectively.



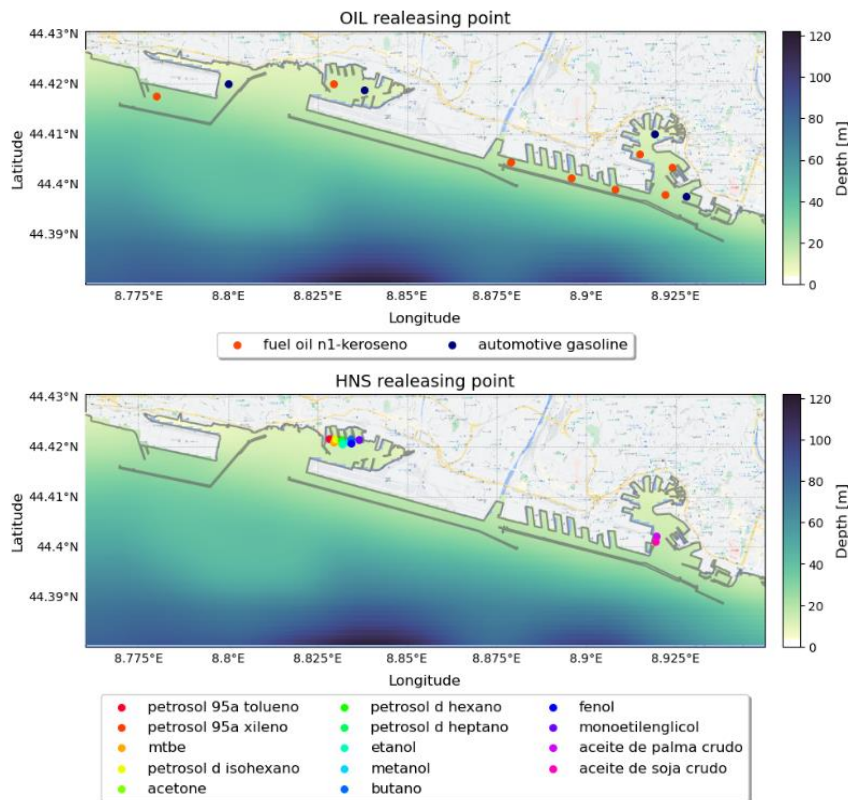


Figure 15 - Releasing positions for oil (top) and HNS (down) spills.

The oil characteristics for each spill point has been established considering the typical oil used as fuel by cargos and large cruises (fuel oil n1-keroseno) and by recreational boat (automotive gasoline). In Table 4 **Errore. L'origine riferimento non è stata trovata.** are shown the properties of these substances, which have been obtained from official sources including the National Centre for Biotechnology Information (NCBI, <https://pubchem.ncbi.nlm.nih.gov/>) and the European Chemicals Agency (ECHA, <https://echa.europa.eu/>). Based on this information, substances have been classified according to their behaviour into the following categories: F: floater; FE: floater/evaporator.



Table 4 – Oil spill points in Genoa.

Terminal	lat	lon	Substance	Type	Volume (m ³)	Behavior	In Teseo (Y/N)	Terminal type
Prà	44,4177	8,78	fuel oil n1-keroseno	Oil	5	FE	Y	channel
Prà	44,42	8,8	automotive gasoline	Oil	5	F	Y	channel
Multedo	44,42	8,8295	fuel oil n1-keroseno	Oil	5	FE	Y	channel
Multedo	44,4189	8,838	automotive gasoline	Oil	5	F	Y	channel
Sampierdarena	44,4044	8,879	fuel oil n1-keroseno	Oil	5	FE	Y	channel
Sampierdarena	44,4013	8,8958	fuel oil n1-keroseno	Oil	5	FE	Y	channel
Sampierdarena	44,39905	8,908	fuel oil n1-keroseno	Oil	5	FE	Y	channel
Porto Antico	44,398	8,922	fuel oil n1-keroseno	Oil	5	FE	Y	manouering area
Porto Antico	44	9	automotive gasoline	Oil	5	F	Y	
Porto Antico	44	8,9239	fuel oil n1-keroseno	Oil	5	FE	Y	dry dock
Porto Antico	44,406	8,915	fuel oil n1-keroseno	Oil	5	FE	Y	porto antico basin
Porto Antico	44,41	8,9192	automotive gasoline	Oil	5	F	Y	porto antico basin

The HNS characteristics for each spill point have been established based on the chemical substances managed in the two chemical deposit in the Port of Genoa, according to the documents provided by the chemical companies, through their websites. In Table 5 are shown the properties of these substances, which have been obtained from official sources including the National Center for Biotechnology Information (NCBI, <https://pubchem.ncbi.nlm.nih.gov/>) and the European Chemicals Agency (ECHA, <https://echa.europa.eu/>). Based on this information, substances have been classified according to their behaviour into the following categories: G: gas; D: dissolver; E: *evaporator*; F: *floaters*; S: *sinker*; DE: *dissolver/evaporator*; ED: *evaporator/dissolver*; FD: *floaters/dissolver*; FE: *floaters/evaporator*; SD: *sinker/dissolver*.





Table 5 – HNS spill points in Genoa.

Terminal	lat	lon	Substance in terminal	Substance	Formula	Volume (m ³)	Behavior	Terminal type
Multedo	44	8,82834	toluene	petrosol 95a tolueno	C7H8	5	FE	deposit of chemicals
Multedo	44	8,82998	xylene	petrosol 95a xileno	C8H10	5	E	deposit of chemicals
Multedo	44	8,8294	methyl ethyl ketone	mtbe	C5H12O	5	SD	deposit of chemicals
Multedo	44	8,82988	methoxypropyl acetate	petrosol d isohecano	C6H12O3	5	E	deposit of chemicals
Multedo	44	8,83165	acetone	acetone	C3H6O	5	SD	deposit of chemicals
Multedo	44	8,83172	hexane	petrosol d hexano	C6H14	5	E	deposit of chemicals
Multedo	44	8,8324	heptane	petrosol d heptano	C7H16	5	E	deposit of chemicals
Multedo	44	8,832	ethanol	etanol	C2H6O	5	D	deposit of chemicals
Multedo	44	8,833799	methanol	metanol	CH4O	5	D	deposit of chemicals
Multedo	44	8,834284	dinitrophenol	fenol	C6H6O	5	SD	deposit of chemicals
Multedo	44	8,8365	ethylene glycol	monoetile glicol	C2H6O2	5	SD	deposit of chemicals
Bettolo	44	8,919624	palm oil	aceite de palma crudo	-	5	F	oil terminal
Bettolo	44	8,919399	soy oil	aceite de soja crudo	C11H9N3 O2Na	5	F	oil terminal

Port of Tripoli (based on Be-Ready project)

According to Be-Ready results, the spill location of the scenarios selected in the Port of Tripoli are the following (see Figure 16):

- 1 point next to the ferry to Turkey station
- 1 point in the small boats and fish market port
- 3 points in the main port and 1 point in the entrance to the port
- 1 point next to the container terminal



UCPM-2022-PP/G.A-101101263-PROMPT



- 1 point where the port expansion is projected (east of the container terminal)
- 4 points in the navigation areas with greater marine traffic
- 3 points in the ship waiting areas
- 1 point next to the International Petroleum Company (highlighted as a possible spill source)

A total of 30 oil spill and 44 HNS spill scenarios has been selected (combination of the aforementioned locations, products and volume), as described in Table 6 and Table 7, respectively.

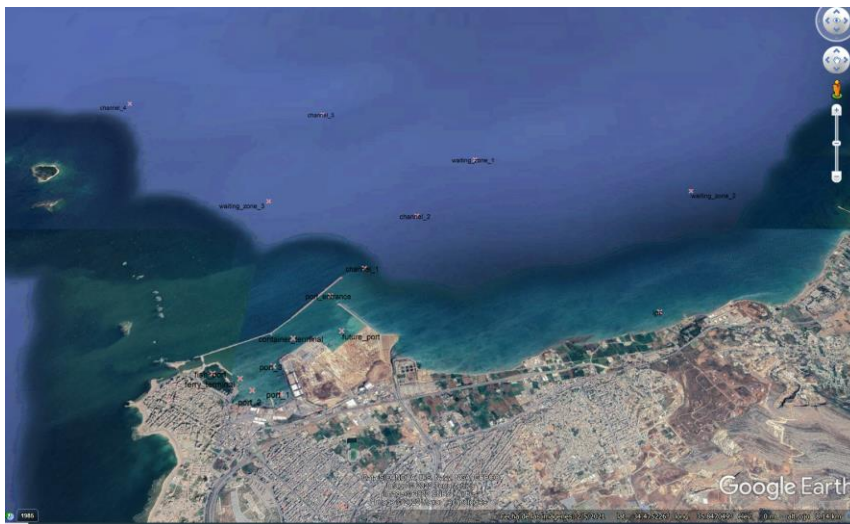


Figure 16 - Location of the spill points in the Port of Tripoli.





Table 6 – Oil spill scenarios selected in the Port of Tripoli.

Spill no.	Point	Ref.	Lat	Long	Substance	Type	Volume [m ³]
1	ferry_terminal	Tasucu Ferry Terminal	35°49'12"	34°27'17"	Fuel Oil IN1-Keroseno	1	5
2	fish_port	Al Mina Fish Port	35°48'55"	34°27'19"	Automotive Gasoline	1	5
3	fish_port	Al Mina Fish Port	35°48'55"	34°27'19"	Fuel Oil IN1-Diesel	1	5
4	port_1	Main Port Southeast	35°49'33"	34°27'08"	Fuel Oil IN1-Keroseno	1	5
5	port_1	Main Port Southeast	35°49'33"	34°27'08"	Fuel Oil IN6	1	5
6	port_2	Main Port Southwest	35°49'18"	34°27'09"	Fuel Oil IN1-Keroseno	1	5
7	port_2	Main Port Southwest	35°49'18"	34°27'09"	Fuel Oil IN6	1	5
8	port_3	Main Port North	35°49'27"	34°27'23"	Fuel Oil IN1-Keroseno	1	5
9	port_3	Main Port North	35°49'27"	34°27'23"	Fuel Oil IN6	1	5
10	container_terminal	Main Port Container Terminal	35°49'35"	34°27'38"	Fuel Oil IN1-Keroseno	1	5
11	port_entrance	Main Port Entrance	35°49'52"	34°28'04"	Fuel Oil IN1-Keroseno	1	5
12	port_entrance	Main Port Entrance	35°49'52"	34°28'04"	Fuel Oil IN6	1	5
13	future_port	Main Port Expansion Zone	35°50'01"	34°27'42"	Fuel Oil IN1-Keroseno	1	5
14	future_port	Main Port Expansion Zone	35°50'01"	34°27'42"	Fuel Oil IN6	1	5
15	channel_1	Channel South	35°50'11"	34°28'22"	Fuel Oil IN1-Keroseno	1	5
16	channel_1	Channel South	35°50'11"	34°28'22"	Fuel Oil IN6	1	5
17	channel_2	Channel Center-South	35°50'42"	34°29'01"	Fuel Oil IN1-Keroseno	1	5
18	channel_2	Channel Center-South	35°50'42"	34°29'01"	Fuel Oil IN6	1	5
19	waiting_zone_1	Waiting Zone Center	35°51'21"	34°29'48"	Fuel Oil IN1-Keroseno	1	5
20	waiting_zone_1	Waiting Zone Center	35°51'21"	34°29'48"	Fuel Oil IN6	1	5
21	channel_3	Channel Center-North	35°49'28"	34°30'31"	Fuel Oil IN1-Keroseno	1	5
22	channel_3	Channel Center-North	35°49'28"	34°30'31"	Fuel Oil IN6	1	5
23	channel_4	Channel Northwest	35°47'00"	34°30'43"	Fuel Oil IN1-Keroseno	1	5
24	channel_4	Channel Northwest	35°47'00"	34°30'43"	Fuel Oil IN6	1	5
25	waiting_zone_2	Waiting Zone East	35°53'42"	34°29'19"	Fuel Oil IN1-Keroseno	1	5
26	waiting_zone_2	Waiting Zone East	35°53'42"	34°29'19"	Fuel Oil IN6	1	5
27	waiting_zone_3	Waiting Zone West	35°49'03"	34°29'12"	Fuel Oil IN1-Keroseno	1	5
28	waiting_zone_3	Waiting Zone West	35°49'03"	34°29'12"	Fuel Oil IN6	1	5
29	ipc	International Petroleum Company	35°52'57"	34°27'53"	Arabian Light	0	5
30	ipc	International Petroleum Company	35°52'57"	34°27'53"	Fuel Oil IN6	1	5





Table 7 – HNS spill scenarios selected in the Port of Tripoli.

Spill no.	Point	Ref.	Lat.	Long.	Substance	SEIC	Volume (m ³)
1	port_1	Main Port Southeast	35489 33"	34272 08"	Etanol	D	5
2	port_1	Main Port Southeast	35489 33"	34272 08"	Binocno	E	5
3	port_1	Main Port Southeast	35489 33"	34272 08"	Cumano	FE	5
4	port_1	Main Port Southeast	35489 33"	34272 08"	Fenol	SD	5
5	port_2	Main Port Southwest	35489 18"	34272 09"	Etanol	D	5
6	port_2	Main Port Southwest	35489 18"	34272 09"	Binocno	E	5
7	port_2	Main Port Southwest	35489 18"	34272 09"	Cumano	FE	5
8	port_2	Main Port Southwest	35489 18"	34272 09"	Fenol	SD	5
9	port_3	Main Port North	35489 27"	34272 23"	Etanol	D	5
10	port_3	Main Port North	35489 27"	34272 23"	Binocno	E	5
11	port_3	Main Port North	35489 27"	34272 23"	Cumano	FE	5
12	port_3	Main Port North	35489 27"	34272 23"	Fenol	SD	5
13	port_entrance	Main Port Entrance	35489 52"	34282 04"	Etanol	D	5
14	port_entrance	Main Port Entrance	35489 52"	34282 04"	Binocno	E	5
15	port_entrance	Main Port Entrance	35489 52"	34282 04"	Cumano	FE	5
16	port_entrance	Main Port Entrance	35489 52"	34282 04"	Fenol	SD	5
17	channel_1	Channel South	35492 11"	34282 22"	Etanol	D	5
18	channel_1	Channel South	35492 11"	34282 22"	Binocno	E	5
19	channel_1	Channel South	35492 11"	34282 22"	Cumano	FE	5
20	channel_1	Channel South	35492 11"	34282 22"	Fenol	SD	5
21	channel_2	Channel Center South	35492 42"	34282 01"	Etanol	D	5
22	channel_2	Channel Center South	35492 42"	34282 01"	Binocno	E	5
23	channel_2	Channel Center South	35492 42"	34282 01"	Cumano	FE	5
24	channel_2	Channel Center South	35492 42"	34282 01"	Fenol	SD	5
25	waiting_zone_1	Waiting Zone Center	35491 21"	34282 48"	Etanol	D	5
26	waiting_zone_1	Waiting Zone Center	35491 21"	34282 48"	Binocno	E	5
27	waiting_zone_1	Waiting Zone Center	35491 21"	34282 48"	Cumano	FE	5
28	waiting_zone_1	Waiting Zone Center	35491 21"	34282 48"	Fenol	SD	5
29	channel_3	Channel Center North	35489 28"	34302 31"	Etanol	D	5
30	channel_3	Channel Center North	35489 28"	34302 31"	Binocno	E	5
31	channel_3	Channel Center North	35489 28"	34302 31"	Cumano	FE	5
32	channel_3	Channel Center North	35489 28"	34302 31"	Fenol	SD	5
33	channel_4	Channel Northwest	35487 00"	34302 43"	Etanol	D	5
34	channel_4	Channel Northwest	35487 00"	34302 43"	Binocno	E	5
35	channel_4	Channel Northwest	35487 00"	34302 43"	Cumano	FE	5
36	channel_4	Channel Northwest	35487 00"	34302 43"	Fenol	SD	5
37	waiting_zone_2	Waiting Zone East	35493 42"	34282 39"	Etanol	D	5
38	waiting_zone_2	Waiting Zone East	35493 42"	34282 39"	Binocno	E	5
39	waiting_zone_2	Waiting Zone East	35493 42"	34282 39"	Cumano	FE	5
40	waiting_zone_2	Waiting Zone East	35493 42"	34282 39"	Fenol	SD	5
41	waiting_zone_3	Waiting Zone West	35489 03"	34282 12"	Etanol	D	5
42	waiting_zone_3	Waiting Zone West	35489 03"	34282 12"	Binocno	E	5
43	waiting_zone_3	Waiting Zone West	35489 03"	34282 12"	Cumano	FE	5
44	waiting_zone_3	Waiting Zone West	35489 03"	34282 12"	Fenol	SD	5

Port of Aqaba (based on Be-Ready project)

According to Be-Ready results, the spill location of the scenarios selected in the Port of Aqaba are the following (see Figure 17):

- 1 point next to the main leisure port and 1 point next to the fish market port.
- 3 points in the main port (north port).
- 2 points in the middle port and 1 point in the ferry terminal right next to it to the south.
- 1 point in the Naval Base.
- 1 point in each of the industrial port terminals.
- 2 points in the new port.
- 4 points in the navigation areas with greater marine traffic.

A total of 29 oil spill and 32 HNS spill scenarios has been selected (combination of the aforementioned locations, products and volume), as described in Table 8 and Table 9, respectively.





Figure 17 - Location of the spill points in the Port of Aqaba.





Table 8 – Oil spill scenarios selected in the Port of Aqaba.

Spill no.	Point	Ref.	Lat.	Long.	Substance	Type	Volume [m ³]	Dens. [kg/m ³]	Mass [kg]
1	leisure_port	Royal Yacht Club	29°31'45.30"N	34°59'49.60"E	Automotive Gasoline	1	5	742	3710
2	leisure_port	Royal Yacht Club	29°31'45.30"N	34°59'49.60"E	Fuel Oil n1-Diesel	1	5	834	4170
3	fishing_port	Fish Market Port	29°31'13.39"N	34°59'56.52"E	Automotive Gasoline	1	5	742	3710
4	fishing_port	Fish Market Port	29°31'13.39"N	34°59'56.52"E	Fuel Oil n1-Diesel	1	5	834	4170
5	main_port_1	Main Port North	29°31'3.90"N	34°59'55.04"E	Light refined oil (Fuel Oil N1-Keroseno)	1	5	816	4080
6	main_port_2	Main Port Center	29°30'51.48"N	34°59'40.87"E	Light refined oil (Fuel Oil N1-Keroseno)	1	5	816	4080
7	main_port_3	Main Port South	29°30'20.76"N	34°59'29.47"E	Light refined oil (Fuel Oil N1-Keroseno)	1	5	816	4080
8	mid_port_1	Middle Port North	29°28'47.48"N	34°58'46.97"E	Light refined oil (Fuel Oil N1-Keroseno)	1	5	816	4080
9	mid_port_2	Middle Port South	29°28'5.23"N	34°58'26.11"E	Light refined oil (Fuel Oil N1-Keroseno)	1	5	816	4080
10	ferry_terminal	Middle Port Ferry Terminal	29°27'39.34"N	34°58'25.88"E	Light refined oil (Fuel Oil N1-Keroseno)	1	5	816	4080
11	naval_base	Royal Jordanian Naval Base	29°23'39.88"N	34°57'47.46"E	Automotive Gasoline	1	5	742	3710
12	naval_base	Royal Jordanian Naval Base	29°23'39.88"N	34°57'47.46"E	Fuel Oil n1-Diesel	1	5	834	4170
13	naval_base	Royal Jordanian Naval Base	29°23'39.88"N	34°57'47.46"E	Light refined oil (Fuel Oil N1-Keroseno)	1	5	816	4080
14	lpg_terminal	Liquefied Petroleum Gas Terminal	29°23'8.27"N	34°57'53.66"E	Light refined oil (Fuel Oil N1-Keroseno)	1	5	816	4080
15	oil_terminal	Oil Terminal	29°22'57.81"N	34°57'46.25"E	Crude oil (Arabian Light)	0	5	869	4345
16	oil_terminal	Oil Terminal	29°22'57.81"N	34°57'46.25"E	Heavy refined oil (Fuel Oil n6)	1	5	979	4895
17	lng_terminal	Liquefied Natural Gas Terminal	29°22'30.36"N	34°57'40.28"E	Light refined oil (Fuel Oil N1-Keroseno)	1	5	816	4080
18	lpgc_terminal	Industrial Terminal	29°22'9.83"N	34°57'32.22"E	Heavy refined oil (Fuel Oil n6)	1	5	979	4895
19	lpgc_terminal	Industrial Terminal	29°22'9.83"N	34°57'32.22"E	Light refined oil (Fuel Oil N1-Keroseno)	1	5	816	4080
20	new_port_1	New Port North	29°21'48.11"N	34°57'38.93"E	Light refined oil (Fuel Oil N1-Keroseno)	1	5	816	4080
21	new_port_2	New Port South	29°21'39.36"N	34°57'49.76"E	Light refined oil (Fuel Oil N1-Keroseno)	1	5	816	4080
22	channel_1	Channel South	29°23'3.68"N	34°54'4.13"E	Light refined oil (Fuel Oil N1-Keroseno)	1	5	816	4080
23	channel_1	Channel South	29°23'3.68"N	34°54'4.13"E	Heavy refined oil (Fuel Oil n6)	1	5	979	4895
24	channel_2	Channel Center-South	29°25'50.04"N	34°56'0.58"E	Light refined oil (Fuel Oil N1-Keroseno)	1	5	816	4080
25	channel_2	Channel Center-South	29°25'50.04"N	34°56'0.58"E	Heavy refined oil (Fuel Oil n6)	1	5	979	4895
26	channel_3	Channel Center-North	29°28'36.12"N	34°57'36.10"E	Light refined oil (Fuel Oil N1-Keroseno)	1	5	816	4080
27	channel_3	Channel Center-North	29°28'36.12"N	34°57'36.10"E	Heavy refined oil (Fuel Oil n6)	1	5	979	4895
28	channel_4	Channel North	29°30'42.29"N	34°58'53.57"E	Light refined oil (Fuel Oil N1-Keroseno)	1	5	816	4080
29	channel_4	Channel North	29°30'42.29"N	34°58'53.57"E	Heavy refined oil (Fuel Oil n6)	1	5	979	4895





Table 9 – HNS spill scenarios selected in the Port of Aqaba.

Spillno.	Point	Ref	Lat	Long	Substance	SEBC	Volume [m ³]	Dens. [kg/m ³]	Mass [kg]
1	main_port_3	Main Port South	29°30'20.76"N	34°59'29.47"E	Etanol	D	5	789,3	3946,5
2	main_port_3	Main Port South	29°30'20.76"N	34°59'29.47"E	Benceno	E	5	879,4	4397
3	main_port_3	Main Port South	29°30'20.76"N	34°59'29.47"E	Cumeno	FE	5	864	4320
4	main_port_3	Main Port South	29°30'20.76"N	34°59'29.47"E	Fenol	SD	5	1071	5355
5	mid_port_1	Middle Port North	29°28'47.48"N	34°58'46.97"E	Etanol	D	5	789,3	3946,5
6	mid_port_1	Middle Port North	29°28'47.48"N	34°58'46.97"E	Benceno	E	5	879,4	4397
7	mid_port_1	Middle Port North	29°28'47.48"N	34°58'46.97"E	Cumeno	FE	5	864	4320
8	mid_port_1	Middle Port North	29°28'47.48"N	34°58'46.97"E	Fenol	SD	5	1071	5355
9	jipc_terminal	Industrial Terminal	29°22'9.83"N	34°57'32.22"E	Etanol	D	5	789,3	3946,5
10	jipc_terminal	Industrial Terminal	29°22'9.83"N	34°57'32.22"E	Benceno	E	5	879,4	4397
11	jipc_terminal	Industrial Terminal	29°22'9.83"N	34°57'32.22"E	Cumeno	FE	5	864	4320
12	jipc_terminal	Industrial Terminal	29°22'9.83"N	34°57'32.22"E	Fenol	SD	5	1071	5355
13	new_port_2	New Port South	29°21'39.36"N	34°57'49.76"E	Etanol	D	5	789,3	3946,5
14	new_port_2	New Port South	29°21'39.36"N	34°57'49.76"E	Benceno	E	5	879,4	4397
15	new_port_2	New Port South	29°21'39.36"N	34°57'49.76"E	Cumeno	FE	5	864	4320
16	new_port_2	New Port South	29°21'39.36"N	34°57'49.76"E	Fenol	SD	5	1071	5355
17	channel_1	Channel South	29°23'3.68"N	34°54'4.13"E	Etanol	D	5	789,3	3946,5
18	channel_1	Channel South	29°23'3.68"N	34°54'4.13"E	Benceno	E	5	879,4	4397
19	channel_1	Channel South	29°23'3.68"N	34°54'4.13"E	Cumeno	FE	5	864	4320
20	channel_1	Channel South	29°23'3.68"N	34°54'4.13"E	Fenol	SD	5	1071	5355
21	channel_2	Channel Center-South	29°25'50.04"N	34°56'0.58"E	Etanol	D	5	789,3	3946,5
22	channel_2	Channel Center-South	29°25'50.04"N	34°56'0.58"E	Benceno	E	5	879,4	4397
23	channel_2	Channel Center-South	29°25'50.04"N	34°56'0.58"E	Cumeno	FE	5	864	4320
24	channel_2	Channel Center-South	29°25'50.04"N	34°56'0.58"E	Fenol	SD	5	1071	5355
25	channel_3	Channel Center-North	29°28'36.12"N	34°57'36.10"E	Etanol	D	5	789,3	3946,5
26	channel_3	Channel Center-North	29°28'36.12"N	34°57'36.10"E	Benceno	E	5	879,4	4397
27	channel_3	Channel Center-North	29°28'36.12"N	34°57'36.10"E	Cumeno	FE	5	864	4320
28	channel_3	Channel Center-North	29°28'36.12"N	34°57'36.10"E	Fenol	SD	5	1071	5355
29	channel_4	Channel North	29°30'42.29"N	34°58'53.57"E	Etanol	D	5	789,3	3946,5
30	channel_4	Channel North	29°30'42.29"N	34°58'53.57"E	Benceno	E	5	879,4	4397
31	channel_4	Channel North	29°30'42.29"N	34°58'53.57"E	Cumeno	FE	5	864	4320
32	channel_4	Channel North	29°30'42.29"N	34°58'53.57"E	Fenol	SD	5	1071	5355

c) Spill simulations and statistical analysis

The simulation of each spill scenario is carried out, for each met-ocean condition (see section 2), using the oil and HNS numerical model TESEO described in section 3.2.1.

Thus, a total of 552 spill simulations have been carried out in the Port of Genoa (combination of 23 metocean conditions, 11 oil scenarios and 13 HNS scenarios), 1850 spill simulations in the Port of Tripoli (combination of 25 metocean conditions, 30 oil scenarios and 44 HNS scenarios) and 1525 spill simulations in the Port of Aqaba (combination of 25 metocean conditions, 29 oil scenarios and 32 HNS scenarios).

The probability of a specific area of being affected by a spill scenario (defined by the spill location, substance and volume) is calculated according to the probabilities of its corresponding met-ocean condition (P^{Ci}). For each Lagrangian simulation, an auxiliary grid is used to count the simulation particles at the surface. The probability of contamination P_{cont} , in the i-th grid cell is obtained as follows:





$$P_{cont} = \sum_{i=1}^{N_c} P^{C_i} \cdot P_i \quad (0,1) \quad (34)$$

where N_c is the number of met-ocean scenarios, P^{C_i} is the probability of occurrence of the met-ocean condition (C_i) and P_i is a binary variable indicating the presence or absence of any particle within cell i :

$$P_i = \begin{cases} 0, & \text{if no particle lies inside the } i\text{-th cell} \\ 1, & \text{if any particle lies inside the } i\text{-th cell} \end{cases}$$

3.2.4.2. Vulnerability

Oil spill vulnerability assessment

The aim of this analysis is to obtain a database that quantifies the vulnerability in the pilot sites to be able to evaluate the risk. The vulnerability assessment is carried out considering the physical, biological and socio-economic resources of the sites by means of different indexes, following the methodology proposed by Abascal et al., 2015; 2022.

- Physical index (P). P is based on ESI (Environmental Sensitivity Index) (Petersen et al., 2002), assesses the potential impact of an oil spill based on the ease of clean-up, depending on the relative exposure to wave energy and the slope of the seabed (beaches, rocks, cliffs and vertical dikes) (see Table 10).

Table 10 - Physical vulnerability levels.

Wave exposure	Coast slope	Physical vulnerability	
Exposed	Cliff or vertical dike	Very low	1
	Rock	Low	2
	Beach		
Semi-exposed	Cliff or vertical dike	Medium	3
	Rock		
	Beach	High	4
Cliff or vertical dike			
Sheltered	Rock	Very high	5
	Beach		
	Cliff or vertical dike		

- Environmental index (E). E is estimated based on the protected species and habitats existing in an area (see Table 11): Conservation Areas (e.g., national and natural parks), Habitats of





Community Interest (e.g., Site of Community Importance (SCI), Special Area of Conservation (SAC), and Special Protection Area (SPA)) and threatened species.

Table 11 - Environmental vulnerability levels.

Protected species/habitats	Environmental vulnerability	
No conservation areas	Low	2
Conservation areas	Medium	3
Non-Priority Special Area of Conservation or Site of Community Importance	High	4
Priority Habitat of Community Interest or Threatened species	Very high	5

- **Socio-economic index (SE).** SE is defined to assess the potential impact of an oil spill based on the duration of the interruption of the socio-economic activities located in the study area (Abascal et al., 2015) (see Table 12).

Table 12 - Socio-economic vulnerability levels.

Activity interruption	Socio-economic vulnerability	
Activity interrupted by a large surface pollution (slick) – Several days of interruption	Very low	1
Activity interrupted by a surface pollution (patches or patties) - Several weeks of interruption	Low	2
Activity interrupted by a surface pollution (tarballs) - Several weeks to months interruption	Medium	3
Activity interrupted by a light surface pollution (diffuse tarballs) - Several months to one-year interruption	High	4
Activity interrupted by invisible trace of oil (dissolve) - One year or more	Very high	5

HNS spill vulnerability assessment

The vulnerability for HNS spills is assessed from a human, environmental and socio-economic point of view:





- **Human index (H).** H is determined considering the different activities performed in each area (fisheries, aquaculture, port areas), as well as the distribution of human settlements and the population vulnerability (see Table 13).

Table 13 - Human vulnerability levels.

Human activities/uses	Human vulnerability	
Without uses/activities	Very low	1
Fisheries, aquaculture areas, port uses	Low	2
Non-populated areas	Medium	3
Populated areas	High	4
Sites with vulnerable population	Very high	5

- **Environmental index (E).** E is estimated, such as for oil spills, based on the protected species and habitats existing in an area (see Table 11): Conservation Areas (e.g., national and natural parks), Habitats of Community Interest (e.g., Site of Community Importance (SCI), Special Area of Conservation (SAC), and Special Protection Area (SPA)) and threatened species.
- **Socio-economic index (SE).** SE is based on the potential impact of water pollution (both surface water and water column) on the main socio-economic activities (Legrand et al., 2017) (see Table 14).

Table 14 - Socio-economic vulnerability levels.

Socio-economic activity	Socio-economic Vulnerability	
Ports	Low	2
Marinas	Medium	3
Aquaculture	High	4
Tourism Recreational beaches	Very high	5

3.2.4.3. Risk

Once the hazard and the vulnerability are known at the study sites, the risk assessment is able to be evaluated by means of the equation:

$$R = H \cdot V$$





As a preliminary step to obtaining risk (R), the hazard values are standardized on 5 levels (see Table 15).

Table 15 - Hazard levels.

Hazard ranges	Hazard level	
0	No hazard	0
0 - 10%	Very low	1
10% - 30%	Low	2
30% - 60%	Medium	3
60% - 100%	High	4

Consecutively, a risk weight (RW) is assigned to each possible result of the product of the hazard level (H) and the different vulnerability indexes (V), as is shown in Table 16.

Table 16 - Risk weights.

H · V	0	1	2	3	4	5	6	8	9	10	12	15	16	20
Risk weight	0	1	2	3	4	5	6	7	8	9	10	11	12	13

Next, the following criteria is applied in order to obtain the standardized risk (R) for each risk weight, which results in the values presented in Table 17.

$$R = \begin{cases} 0 & \text{if } RW = 0 \\ \text{round} \left(\frac{RW - \min(RW)}{\max(RW) - \min(RW)} \cdot (n\text{classes} - 1) + 1 \right) & \text{if } RW \neq 0 \end{cases}$$

Where

- *round* is a function that rounds the result to the nearest integer
- $\min(RW)$ is the minimum non-zero risk weight (1 in this case)
- $\max(RW)$ is the maximum risk weight (13 in this case)
- *nclasses* is the number of desired standardized risk levels (5 in this case)





Table 17 - Standardized risks.

H · V	0	1	2	3	4	5	6	8	9	10	12	15	16	20
Risk weight	0	1	2	3	4	5	6	7	8	9	10	11	12	13
Standardized risk	0	1	1	2	2	2	3	3	3	4	4	4	5	5

As a result, 5 standardized risk levels (R) can be determined by multiplying the hazard level and the vulnerability (see Table 18).

Table 18 – Risk levels.

H · V	Risk	
0	No risk	0
1 - 2	Very low	1
3 - 5	Low	2
6 - 9	Medium	3
10 - 15	High	4
16 - 20	Very high	5

3.2.4.4. Results

The Risk Assessment model provides the following results for oil and HNS spills in the marine environment:

For oil spills:

- i. Hazard maps for each spill scenario.
- ii. Estimated time of arrival maps for each spill scenario.
- iii. Vulnerability maps: Physical, Environmental and Socioeconomic vulnerability maps.
- iv. Risk maps: Physical, Environmental and Socioeconomic risk maps.

For HNS spills:

- i. Hazard maps for each spill scenario.
- ii. Estimated time of arrival maps for each spill scenario.
- iii. Vulnerability maps: Human, Environmental and Socioeconomic vulnerability maps.





iv. Risk maps: Human, Environmental and Socioeconomic risk maps.

The outputs will be available within the DSS platform.

As mentioned in section 1.2 and Figure 5, the risk from oil and chemical spills in the marine environment is estimated in the port of Genoa as a new implementation in the framework of PROMPT project. In addition, the risk assessment carried out in Aqaba and Tripoli in the framework of the BE-READY project will be updated taking into account the new high-resolution wind databases developed in PROMPT.

As an example, some results obtained after applying in the port of Genoa the methodology described above are shown.

- **Hazard:**

Figure 18 shows an example of the probability of contamination and the Estimation Time of Arrival (ETA) obtained for an oil and HNS scenario in the Port of Genoa. As mentioned, a post-processed analysis of the scenarios modelled by TESEO allows to evaluate the Estimation Time of Arrival, defined as the time after which the slick reaches a particular area; and the Hazard, defined as the probability that the slick reaches a certain area. The two descriptors are plotted in Figure 18 both for a HNS spill (Petrosol 95a Toluene, left panels) and for an oil spill (automotive gasoline, right panels). The HNS spill never goes out of the port in the 23 scenarios analysed due to the fact that Petrosol 95a Toluene is a very volatile substance. For example, in the first scenario, after the first 4 hours about 80% of the substance is evaporated, while the rest gets stuck on the port's barriers. As for the oil spill, there are two scenarios in which the slick leaves the port and could potentially damage the surrounding marine environment, but with a very low hazard, or probability of occurring. In this case and similar to the HNS spill, for the first scenario, the oil slick takes about 2 hours to evaporate or get beached.



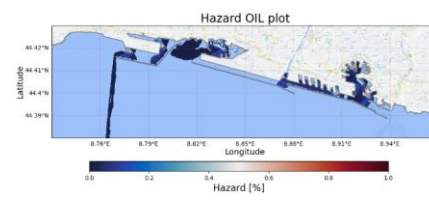
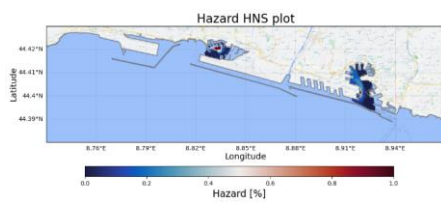
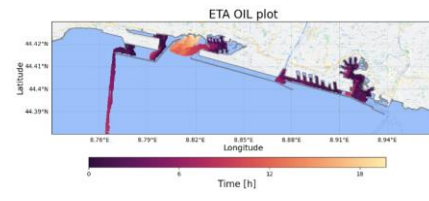
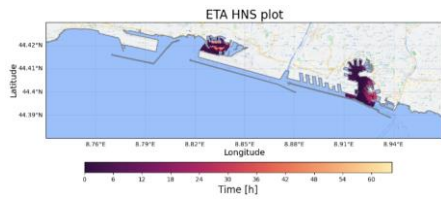


Figure 18 - ETA and hazard map for the HNS (on the left), and for the Oil (on the right).





- **Vulnerability:**

As an example, two of the vulnerability indexes obtained in the Port of Genoa are shown, the physical index for oil spills (Figure 19) and the environmental index for oil and HNS spills (Figure 20).



Figure 19 - Physical vulnerability index for water pollution from OIL spills in the Port of Genoa.





Figure 20 - Environmental vulnerability index for water pollution from OIL/HNS spills in the Port of Genoa.

3.3. Atmospheric pollution modelling

The project involved conducting atmospheric dispersion simulations using the HYSPLIT (Hybrid Single-Particle Lagrangian Integrated Trajectory) model. HYSPLIT, developed by NOAA, is widely used for simulating the transport and dispersion of airborne particles and pollutants, making it an ideal tool for this phase of the project.

3.3.1. Model description

HYSPLIT (Hybrid Single-Particle Lagrangian Integrated Trajectory) is one of the most widely used atmospheric dispersion and trajectory models in the world. Developed and maintained by NOAA's Air Resources Laboratory (ARL), HYSPLIT has become a standard tool for simulating the transport, dispersion, deposition, and chemical transformation of



pollutants, particles, and gases in the atmosphere. Its flexible and user-friendly nature allows for a wide range of applications, from forecasting air pollution events to studying long-range transport of atmospheric contaminants.

HYSPLIT is a hybrid model, combining **Lagrangian** and **Eulerian** approaches to provide high accuracy in tracking and predicting the dispersion of particles in the atmosphere. The model can compute the trajectories of individual air parcels (Lagrangian approach) or simulate the spread of pollutant concentrations on a grid (Eulerian approach), depending on the user's needs. This hybrid capability makes HYSPLIT highly versatile and capable of handling a wide range of atmospheric dispersion problems.

Key features of the HYSPLIT model include:

1. **Hybrid Modeling Approach:** HYSPLIT's core strength is its ability to simulate both the trajectory of particles as they move through the atmosphere and their dispersion across a grid, offering flexibility for different types of atmospheric studies.
2. **Pollutant Transport and Dispersion:** HYSPLIT tracks the transport of pollutants through the atmosphere based on meteorological data, simulating how particles or gases are carried by winds, deposited, or chemically transformed during their travel.
3. **Deposition and Wet Scavenging:** The model includes mechanisms for **dry deposition** (where pollutants settle on surfaces) and **wet deposition** (where pollutants are removed from the atmosphere by precipitation). This is crucial for studying the environmental impacts of contaminants.
4. **Particle and Concentration Modeling:** HYSPLIT can simulate pollutant dispersion as a collection of individual particles or as a concentration field on a predefined grid. This flexibility allows the model to adapt to various spatial scales, from local to global.
5. **Backward and Forward Trajectories:** The model can compute both forward and backward trajectories. Forward trajectories predict the movement of pollutants or particles from a specific source, while backward trajectories can help trace the origin of pollutants observed at a specific location.

HYSPLIT is structured to allow flexibility in both input and output data handling, making it compatible with a variety of meteorological datasets. It uses pre-processed meteorological input data (usually provided in formats like **GRIB**, **NetCDF**, or **ARL** files) to drive the model. The transport and dispersion calculations are then performed in a stepwise fashion over time, based on wind speed, turbulence, and other atmospheric parameters from these meteorological datasets.



UCPM-2022-PP/G.A-101101263-PROMPT



The model operates on a **3D Lagrangian particle tracking system**, which calculates the trajectory of air parcels by integrating their position over time, using wind fields from input data. This system simulates the turbulent movement of particles as they are transported by atmospheric currents. Additionally, the **Eulerian grid approach** allows HYSPLIT to calculate pollutant concentrations over a specific geographic area, making it particularly useful for regional or global-scale studies.

1. Lagrangian Approach:

- In the Lagrangian framework, HYSPLIT models the transport of air parcels by treating them as individual particles that move through space and time. This method is particularly useful for tracing pollutant plumes or determining the path of air masses over time.

2. Eulerian Approach:

- The Eulerian method divides the atmosphere into grid cells, within which pollutant concentrations are calculated at each time step. This approach is more suitable for applications where spatial distribution and concentration of pollutants across a region are of interest, such as air quality modeling or long-range transport of particles.

Meteorological Inputs

The performance and accuracy of HYSPLIT depend largely on the quality of the meteorological input data used to drive the model. HYSPLIT typically requires meteorological data that include 3D wind fields, temperature, humidity, and other variables that influence particle movement and atmospheric mixing. The most commonly used meteorological datasets for HYSPLIT simulations include:

- **NCEP GFS (Global Forecast System):** One of the primary global weather forecasting models, providing high-resolution data used for global simulations.
- **WRF-ARW (Weather Research and Forecasting - Advanced Research WRF):** Often used for regional and high-resolution simulations, as WRF outputs can be pre-processed and converted into HYSPLIT-compatible formats.
- **ECMWF (European Centre for Medium-Range Weather Forecasts):** Another source of global weather data, known for its accuracy and high spatial resolution.





The meteorological data is processed using NOAA's preprocessor tools like **ARW2ARL**, which converts WRF-ARW output into a format that HYSPLIT can use. This pre-processing step is crucial for integrating high-resolution weather data into HYSPLIT simulations.

Deposition and Removal Processes

One of HYSPLIT's core strengths is its ability to simulate deposition processes that remove pollutants from the atmosphere. These include:

- **Dry Deposition:** The removal of particles or gases through direct contact with surfaces (e.g., vegetation, buildings, or the ground).
- **Wet Deposition:** The removal of pollutants through precipitation, where particles or gases are washed out of the atmosphere by rain, snow, or fog. HYSPLIT incorporates wet scavenging processes, making it ideal for studying the fate of pollutants in regions with significant precipitation.

3.3.2. Model implementation

HYSPLIT was configured to simulate pollutant dispersion in both the Aqaba and Tripoli regions. The setup involved specifying the emission sources, pollutant types, and release points based on the scenarios identified in the project. This configuration ensured that the model accurately represented the behavior of pollutants under different atmospheric conditions. Key configuration steps included:

- Defining Emission Scenarios: Various pollutant emission scenarios were modeled, reflecting both natural and anthropogenic sources.
- Meteorological Forcing: The ARL files generated from WRF provided the meteorological inputs necessary to simulate how pollutants would be transported and dispersed by the wind, turbulence, and other atmospheric processes.

Generation of Meteorological Input Files

To drive the HYSPLIT simulations, it was necessary to convert the WRF outputs into a format compatible with the HYSPLIT model. This was achieved using NOAA's arw2arl preprocessor, which converts WRF-ARW outputs (in NetCDF format) into ARL (Air Resources Laboratory) files. These files contained the meteorological variables needed to run the HYSPLIT simulations, including wind fields and temperature. The ARL files played a pivotal role in integrating high-resolution meteorological data from WRF into the HYSPLIT model, ensuring accurate atmospheric dispersion simulations under the predefined scenarios.





Simulation Runs and Postprocessing

Multiple HYSPLIT simulations were executed for each meteorological scenario, using different pollutants and emission levels in line with IH Cantabria's data, generating detailed concentration and deposition maps that showed how pollutants dispersed over time within the target regions. These outputs were then postprocessed according to the TESEO platform's specifications, ensuring that the results were compatible for further analysis.

3.3.2.1. Coupling between TESEO and HYSPLIT

The results of TESEO simulations provide the necessary data to feed HYSPLIT emission source points. This coupling between the models has been made based on the following variables:

- The temporal evolution of the centre of mass of the oil slick
- The temporal evolution of the mass evaporated from the slick to the atmosphere
- The temporal evolution of the slick area

Based on these three variables, a postprocessing has been developed to generate an EMITIME file (emissions file) for the HYSPLIT model. This allows the definition of a source point of emission with a specific area that can vary its location, area and mass emission ratio in time. Thus, the behaviour of the emission derived from a slick can be characterized and the produced evaporation of chemicals can be simulated considering the variability of the source, in this case, a slick that varies its area, location and ratio of mass emission in time.

3.3.3. On-demand forecast modelling

On-demand forecast modelling of the pollutant evaporated from the chemical slick to the atmosphere will be automatically triggered. Once the marine pollution simulation requested by the user ends, PROMPT DSS will detect if the chemical spill is a candidate to produce a toxic emission into the atmosphere. If it is, a pop-up window will warn the user of this fact and ask him if he wants to launch the atmospheric pollutant model (HYSPLIT) see Figure 21.



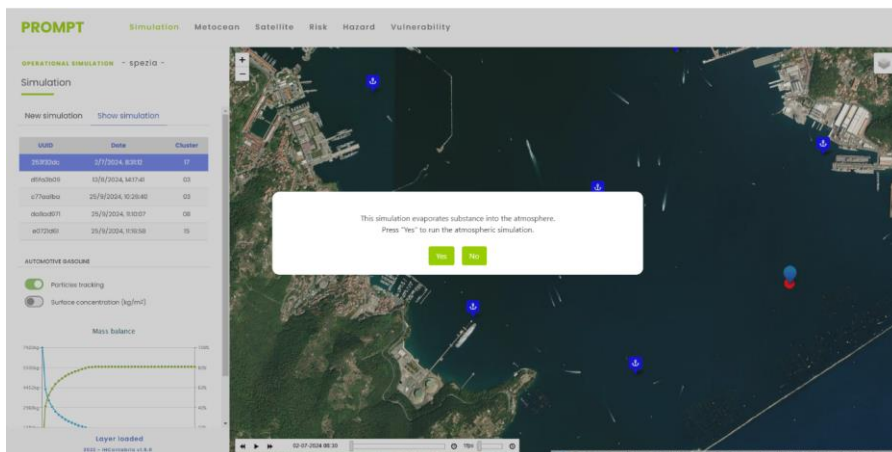


Figure 21 - Pop-up window to launch atmospheric pollution simulation of the evaporated part of the substance

Automatically, if the user decides to launch the simulation, a request will be sent to the IHCantabria server that hosted the HYSPLIT API to run this simulation. In this case, the user does not need to define any parameter of the simulation, the simulation will be carried out with the metocean scenario (cluster) defined in the marine pollution simulation as the configuration of the chemical and the emissions that will be post-process from the TESEO results as commented in section 3.2.2.3.

The results of the Atmospheric pollutant simulation will be the concentration maps of the pollutant between 0 m and 10 m and between 0 m and 50 m, over the mean sea level.



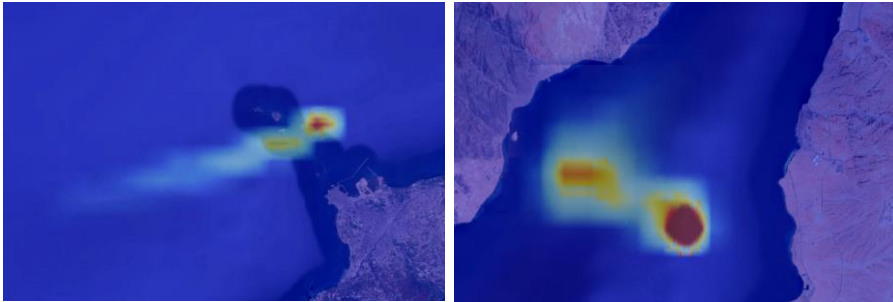


Figure 22 - Example of pollutant concentration between 0 and 10 m over the sea surface at Tripoli (left) and Aqaba (right) port area

3.3.4. Risk assessment methodology

The proposed methodology (see Figure 11) allows to determine the risk in the atmospheric environment of a specific area affected by an HNS spill following the expression $R = H \cdot V$, described in section 0. The methodology is applied in the Port of Tripoli and the Port of Aqaba.

3.3.4.1. Hazard

As described in section 3.2.4.1, the hazard is carried out by the statistical analysis of a hypothetical HNS spill database generated from the selection of different meteocean and spill scenarios, which are then modelled in two steps: (1) marine modelling by TESEO, and (2) atmospheric modelling by HYSPLIT using as input data the TESEO output values for substances that evaporate.

In this case, the HNS spill scenario is the same as that shown for marine pollution in Table 7 for Tripoli and Table 9 for Aqaba, but taking into account only the scenarios associated with substances that can evaporate. Thus, a total of 550 (25 x 22) and 400 (25 x 16) spill simulations will be carried out in Tripoli and Aqaba, respectively.

Based on this database, the probability of a specific area of being affected by the atmospheric pollution will be calculated according to the methodology described in section 3.2.4.1.





3.3.4.2. Vulnerability

The vulnerability for HNS spills in the atmospheric environment, as well as in the marine environment, is assessed from a human, environmental and socio-economic point of view, following the steps described in section 3.2.4.2, but extending the application area of the methodology, due to air pollution can also affect the land area.

3.3.4.3. Risk

Once the hazard and the vulnerability are known at the study sites, the risk assessment is able to be evaluated by following the steps described in section 3.2.4.3.

3.3.4.4. Results

The Risk Assessment model will provide the following results for HNS spills in the atmospheric environment:

- i. Hazard maps for each spill scenario.
- ii. Estimated time of arrival maps for each spill scenario.
- iii. Vulnerability maps: Human, Environmental and Socioeconomic vulnerability maps.
- iv. Risk maps: Human, Environmental and Socioeconomic risk maps.

The outputs will be available within the DSS platform.

As mentioned in section 1.2 and Figure 5, in the framework of this project, the risk from chemical spills in the atmospheric environment has been estimated in Aqaba and Tripoli, using as input data for HYSPLIT the results of the new TESEO simulations with the new high-resolution winds.





4. REFERENCES

- Abascal, A.J., Castanedo, S., Gutierrez, A.D., Comerma, E., Medina, R., Losada, I.J., 2007. TESEO, an Operational System for Simulating Oil Spills Trajectories and Fate Processes. Proceedings of Seventeenth International Offshore Ocean and Polar Engineering Conference. The International Society of Offshore Ocean and Polar Engineering, Lisbon, ISOPE, 3, 1751-1758.
- Abascal, A.J., Castanedo, S., Medina, R., Liste, M., 2010. Analysis of the reliability of a statistical oil spill response model. *Mar. Pollut. Bull.* 60 (11), 2099 - 2110.
- Abascal, A.J., Castanedo, S., Nuñez, P., Cardenas, M., Perez-Diaz, B., Medina, R., 2015. A high resolution oil spill risk assessment system at Santander Bay (Spain), *Interspill 2015*, Amsterdam (Netherlands).
- Abascal, A.J., Castanedo, S., Nuñez, P., Mellor, A., Clements, A., Pérez, B., Cárdenas, M., Chiri, H., Medina, R., 2017a. A high-resolution operational forecast system for oil spill response in Belfast Lough, *Marine Pollution Bulletin*, 114, 302-314.
- Abascal, A.J., Sanchez, J., Chiri, H., Ferrer, M.I., Cárdenas, M., Gallego, A., Castanedo, S., Medina, R., Alonso-Martirena, A., Berx, B., Turrell, W.R., Hughes, S.L., 2017b. Operational oil spill trajectory modelling using HF radar currents: a northwest European continental shelf case study. *Mar. Pollut. Bull.* 119, 336–350. <https://doi.org/10.1016/j.marpolbul.2017.04.010>.
- Abascal, A.J., Gonzalez, M., Aragón, G., Largo, A.M., Lamothe, B., Pedraz, L., Pérez-Díaz, B., de los Ríos, A., Martínez, A., Bárcena, J.F., García, J., García, A., Puente, A., Fernández, F., Medina, R., 2022. A Web-Gis operational system for the risk management of marine and atmospheric pollution from hazardous and noxious substances (HNS) spills in harbour areas, *Interspill 2022*, Amsterdam (Netherlands).
- ASCE, 1996. State-of-the-art review of modeling transport and fate of oil spills, ASCE Committee on Modeling Oil Spills. Water Resources Engineering Division. *Journal of Hydraulic Engineering*, 122(11), 594-609.
- Barker, C.H., Galt, J.A., 2000. Analysis of methods used in spill response planning: trajectory analysis planner TAP II. *Spill Sci. Technol. Bull.* 6 (2), 145–152.
- Berry, A., Dabrowski, T., Lyons, K., 2012. The oil spill model OILTRANS and its application to the Celtic Sea. *Marine Pollution Bulletin*, Vol. 64, pp. 2489–2501.
- Buchanan, I., Hurford, N., 1988. Methods for predicting the physical changes of oil spilled at sea. *Oil and Chemical Pollution*, Vol. 4, No. 4, pp. 311-328.





- Brighton, P.W.M., 1985. Evaporation from a plane liquid surface into a turbulent boundary layer. *J. Fluid Mechanics* 159:323-345.
- Brighton, P.W.M., 1990. Further verification of a theory for mass and heat transfer from evaporating pools. *J. Hazardous Materials* 23:215-234.
- Comerma, E., 2004. Modelado numérico de la deriva y envejecimiento de los hidrocarburos vertidos al mar. Aplicación operacional en la lucha contra las mareas negras. Tesis doctoral, Universitat Politècnica de Catalunya.
- Chiri, H., Abascal, A.J., Castanedo, S., 2020. Deep oil spill hazard assessment based on spatio-temporal met-ocean patterns, *Marine Pollution Bulletin*, 154, 10.1016/j.marpolbul.2020.111123. IF(2020): 5.553, D1 (3/110).
- Fay, J., 1971. Physical processes in the spread of oil on a water surface. Proc. of the Jount Conf. on Prevention and Control of Oil Spill. American Petroleum Institute, Washington, DC, pp. 463-467.
- Fernandes (2014). Activity 3. Task3.3.2: Technical & Scientific Manual - MOHID HNS (Chemical) Spill Module. Report. ARCOPOLPlus. Improving maritime safety and Atlantic Regions' coastal pollution response through technology transfer, training and Innovation.
- Galt, J.A., Payton, D.L., 1999. Development of quantitative methods for spill response planning: a trajectory analysis planner. *Spill Sci. Technol. Bull.* 5 (1), 17–28.
- Hayduk, W., Laudie, H., 1974. Prediction of Diffusion Coefficients for Non-electrolytes in Dilute Aqueous Solutions, *Jour. AIChE*, 28, 611.
- Hunter, J.R., Craig, P.D., Phillips, H.E., 1993. On the use of random walk models with spatially variable diffusivity. *J. Comp. Phys.*, Vol. 106, pp. 366-376.
- Kawamura, P. I., Mackay, D., 1987. The evaporation of volatile liquids. *J. Hazardous Materials* 15:343-364.
- Kolluru, V.S., 1992. Influence of Number of Spilllets on Spill Model Predictions. Applied Science Associates Internal Report
- Legrand S., F. Poncet, L. Aprin, V. Parthenay, E. Donnay, G. Carvalho, S. Chataing-Pariaud, G. Dusserre, V. Gouriou, S. Le Floch, P. Le Guerroue, Y.-H. Hellouvy, F. Heymes, F. Ovidio, S. Orsi, J.Ozer, K. Parmentier, R. Poisvert, E. Poupon, R. Ramel, R. Schallier, P. Slangen, A. Thomas, V. Tsigourakos, M. Van Cappellen and N. Youdjou (2017) "Mapping Environmental and Socio-Economic Vulnerability to HNS Maritime Pollution", HNS-MS final report, part III, 122 pp





- Lehr, W.J., 2001. Review of modeling procedures for oil spill weathering behavior. Oil Spill Modelling and Processes, C. A. Brebbia Ed., WIT Press, pp. 51-90.
- Mackay, D., Matsugu, R.S., 1973. Evaporation rates of liquid hydrocarbon spills on land and water. Can. J. Chem. Eng. 51:434-439.
- Mackay D., Leinonen P.J., 1977. Mathematical model of the behaviour of oil spills on water with natural and chemical dispersion. – Rapport technique n° EPS-3-EC-77-19, Fisheries and Environmental Canada,
- Mackay, D., Paterson, S., Trudel, K., 1980. A Mathematical Model of Oil Spill Behaviour. Environmental Protection Service, Fisheries and Environment Canada, EE-7, 39p.
- Mackay, D., Paterson S., Nadeau, S., 1980. Calculation of the evaporation rate of volatile liquids. Proc. of the National Conference on Control of Hazardous Material Spills, Louisville, KY, pp. 361-367.
- Mackay, D., Shiu, W.Y., Hossain, K., Stiver, W., McCurdy, D., Petterson, S., Tebeau, P. A., 1983. Development and Calibration of an Oil Spill Behavior Model, Report No. CG-D-27-83, United States Coast Guard Office of Research and Development, Groton, Conn., USA.
- NOAA, 1994. ADIOS. Automated Data Inquiry for Oil Spills. User's Manual (see 1.1). NOAA/Hazardous Materials Response and Assessment Division, Seattle, Washington.
- Petersen, J., Michel, J., Zengel, S., White, M., Lord, C., Plank, C., 2002. Environmental Sensitivity Index Guidelines, Version 3.0.
- Rasmussen, D., 1985. Oil spill modelling - a tool for cleanup operations. Proc. 1985 Oil Spill Conf., American Petroleum Institute, Washington, D.C., pp. 243-249.
- Reed, M., Gundlach, E., y Kana, T., 1989. A coastal zone oil spill model: development and sensitivity studies. Oil and Chemical Pollution, Vol. 5, No. 6, pp. 451-476.
- Reynolds, R. M., 1992. ALOHA™ (Areal Locations of Hazardous Atmospheres) 5.0 theoretical description. NOAA Tech. Memo. NOS ORCA-65. National Oceanic and Atmospheric Administration/Hazardous Materials Response and Assessment Division. Seattle, WA.
- Sebastiao, P., and Guedes Soares, C., 1995. Modeling the Fate of Oil Spills at Sea. Spill Science and Technology Bulletin, Vol.2, No. 2/3, pp. 121-131.
- Sotillo, M.G., E. Alvarez Fanjul, S. Castanedo., A.J. Abascal, J. Menendez, R. Olivella, E. García-Ladona, M. Ruiz-Villareal, J. Conde, M. Gómez, P. Conde, A.D. Gutierrez, and R. Medina, "Towards an Operational System for Oil Spill Forecast in the Spanish Waters: Initial Developments and Implementation Test", Marine Pollution Bulletin, 56(4):686-703, 2008.





Stiver, W. & Mackay, D., 1984. Evaporation Rate of Spills of Hydrocarbons and Petroleum Mixtures. Environment Science & Technology, Vol. 18, pp. 834-840.

Thibodeaux, L.G., 1979. Chemodynamics: environmental movement of chemicals in air, water, and soil, New York, John Wiley and Sons.



UCPM-2022-PP/G.A-101101263-PROMPT